

Reionization and dark matter decay

Isabel M. Oldengott, Daniel Boriero and Dominik J. Schwarz

Fakultät für Physik, Bielefeld University, D-33501 Bielefeld, Germany

E-mail: ioldengott@physik.uni-bielefeld.de, boriero@physik.uni-bielefeld.de,
dschwarz@physik.uni-bielefeld.de

Abstract. Cosmic reionization and dark matter decay can impact observations of the cosmic microwave sky in a similar way. A simultaneous study of both effects is required to constrain unstable dark matter from cosmic microwave background observations. We compare two reionization models with and without dark matter decay. We find that a reionization model that fits also data from quasars and star forming galaxies results in tighter constraints on the reionization optical depth τ_{reio} , but weaker constraints on the spectral index n_s than the conventional parametrization. We use the Planck 2015 data to constrain the effective decay rate of dark matter to $\Gamma_{\text{eff}} < 2.9 \times 10^{-25}/\text{s}$ at 95% C.L. This limit is robust and model independent. It holds for any type of decaying dark matter and it depends only weakly on the chosen parametrization of astrophysical reionization. For light dark matter particles that decay exclusively into electromagnetic components this implies a limit of $\Gamma < 5.3 \times 10^{-26}/\text{s}$ at 95% C.L. Specifying the decay channels, we apply our result to the case of keV-mass sterile neutrinos as dark matter candidates and obtain constraints on their mixing angle and mass, which are comparable to the ones from the diffuse X-ray background.

Contents

1	Introduction	1
2	Astrophysical reionization	2
2.1	Evolution of the free electron fraction	2
2.2	Impact of astrophysical reionization on CMB angular power spectra	5
3	Dark matter decay and cosmic reionization	7
3.1	Dark matter decay	7
3.2	Energy deposition from dark matter decay	8
3.3	Reionization from dark matter decay	9
3.4	Impact of dark matter decay on CMB angular power spectra	11
4	Constraints from CMB observations	12
4.1	Model fitting and comparison	12
4.2	Comparison of astrophysical reionization models	14
4.3	Limits on dark matter decay rate	15
4.4	Constraints on sterile neutrino dark matter	18
5	Conclusions	20
6	Acknowledgements	21
A	Smoothness of visibility function	21
B	Optical depth prior	23

1 Introduction

The universe is highly ionized today, although it was filled by cold gas of hydrogen and helium after the decoupling of photons. Evidence for reionization stems from observations of the spectra of distant quasars that show only a few absorption lines bluewards of the Lyman- α line in the quasar's rest frame. These absorption lines form the so-called Lyman- α forest can be understood as the fingerprints of neutral hydrogen clouds in the intergalactic medium. Already a very small amount of neutral hydrogen (fraction of $\sim 10^{-3}$) is sufficient to entirely suppress the quasar spectra. Hence, the fact that we still observe *any* flux of quasars with $z \lesssim 6$ bluewards of the Lyman alpha line implies that the amount of neutral hydrogen must be very low and consequently the universe is ionized at $z \lesssim 6$.

The observation of the Gunn-Peterson trough [1] (the absence of quasar radiation bluewards of the Lyman- α line) for the highest redshift quasars [2] furthermore indicates that the transition from a neutral to an ionized state happened at $z \sim 6$.

A direct observation of the epoch of reionization could be obtained by means of the 21 cm transition of hydrogen [3, 4]. Instruments like the Low Frequency Array (LOFAR) [5], the Precision Array for Probing the Epoch of Reionization (PAPER) [6] or the Murchison Widefield Array (MWA) [7] are trying to detect the 21 cm brightness temperature fluctuation.

The Experiment to Detect the Global EoR Signature (EDGES) could provide a lower limit on the width of reionization [8].

Another probe of reionization is the cosmic microwave background (CMB) [9, 10]. Reionization increases the number of free electrons, on which some of the CMB photons scatter. This results in a suppression of the temperature and polarization angular power spectra at small scales, but reionization also serves as a source of polarization at the largest angular scales resulting in a very characteristic bump.

Reionization is believed to be caused by the first appearance of luminous extreme UV ($\gtrsim 10$ eV) emitting objects such as heavy stars and quasars [11, 12]. The details of the astrophysical reionization at $z \sim 6$ are not yet well understood and are subject to analytical [13–15] and complicated numerical simulations [16, 17].

Due to its dependence on the free electron fraction, the CMB is also sensitive to any other source of reionization, especially the decay or annihilation of dark matter (DM). This opens the very appealing possibility to obtain constraints on DM properties like its decay or annihilation rate. Various works have studied the impact of DM annihilation on the CMB, e.g. [18–24], the list of literature on DM decay is in contrast surprisingly shorter, e.g. [25–29]. Others also studied the astrophysical effects (not related to the CMB) of annihilating and decaying dark matter on the reionization history [30–33].

In this work, we study how model assumptions on astrophysical reionization affect the inferred values of the amplitude of primordial scalar perturbations A_s , their spectral index n_s , and the DM decay rate Γ from CMB temperature and polarization measurements.

We derive constraints on the DM decay rate from the Planck 2015 data [24]. These constraints are in particular applicable for warm DM candidates such as keV sterile neutrinos [34], which were recently reported to be observed with masses of ~ 7 keV [35, 36]. We thereby also include modifications to the CosmoRec code [37, 38] that are necessary to model DM decay realistically, but which we believe have been missed out in previous works [22, 29].

Our work is organised as follows. In section 2 we introduce two different parametrizations for the free electron fraction during reionization by means of astrophysical processes – the parametrization used in the CAMB code and a new parametrization proposed by [39] based on observations of quasars and star forming galaxies. In section 3 we discuss the decay of DM as an alternative source of reionization and its potential impact on the CMB. We present and discuss the results of our cosmological data analysis in section 4 and conclude in section 5. Details on the numerical implementation can be found in the appendix A and an aspect of the prior distributions of the Bayesian inference problem are discussed in appendix B.

2 Astrophysical reionization

2.1 Evolution of the free electron fraction

The evolution of the free electron fraction $x_e = n_e/n_H$ in an isotropic and homogenous universe is calculated by recombination codes like CosmoRec [37, 38] that take into account multi-level excitations of hydrogen besides radiative transfer corrections of its recombination rate. Whereas helium recombines to HeII at $z \simeq 4000$ and to HeI at $z \simeq 1000$, hydrogen remains ionized until $z \simeq 900$. Due to the decrease of temperature its recombination rate finally exceeds the photoionization rate of excited hydrogen atoms and x_e rapidly decreases to a residual value of the order 10^{-4} , see figure 1. Afterwards, the free electron fraction is

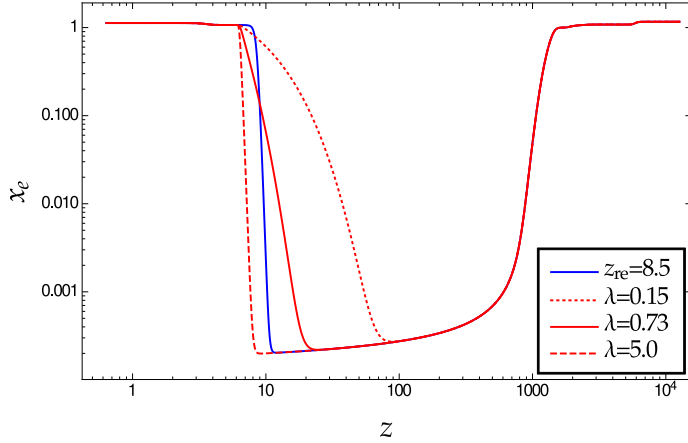


Figure 1: Evolution of the free electron fraction x_e for different models of astrophysical reionization. At high redshifts we show the fraction of free electrons as obtained by means of the CosmoRec code. For intermediate redshifts the blue line shows the parametrization (2.1) as used by the CAMB code and in the Planck 2015 data analysis (blue line). It is compared to the empirical parametrization (2.5) (red lines) for three different values of the model parameter λ .

believed to smoothly continue to decrease until the onset of reionization by astrophysical sources at $z \sim 10$.

For the purpose of CMB analysis the history of astrophysical reionization can be parametrized by a model for the evolution of the free electron fraction. Since the details of the astrophysical processes that cause cosmic reionization are still widely unknown, CAMB models $x_e(z)$ during astrophysical reionization as a smooth, step-like function,

$$x_e(z)|_{\text{CAMB}} = \frac{1.08}{2} \left[1 + \tanh \left(\frac{(1+z_{\text{re}})^{3/2} - (1+z)^{3/2}}{\Delta_z} \right) \right]. \quad (2.1)$$

Here, z_{re} describes the redshift of reionization, i.e. the redshift at which half of the electrons are free and Δ_z quantifies the width of the transition. Typically, cosmological data analysis uses $\Delta_z = 0.5$ per default.

By defining the free electron fraction as $x_e \equiv n_e/n_{\text{H}}$ the numerator counts *all* free electrons, whereas the denominator only counts hydrogen nuclei. Therefore, x_e takes the asymptotic value of ~ 1.08 assuming full ionization of hydrogen plus single ionization of helium and ~ 1.16 assuming additionally double ionization of helium,

$$x_e \equiv \frac{n_e}{n_{\text{H}}} = \frac{n_{e,\text{HIII}}}{n_{\text{H}}} + \frac{n_{e,\text{HeII}}}{n_{\text{H}}} + \frac{n_{e,\text{HeIII}}}{n_{\text{H}}} \quad (2.2)$$

$\xrightarrow{\text{compl. reion.}} 1.0 + 0.08 + 0.08.$

Since normal stellar populations produce only very few photons with energies above 54.4 eV, the second ionization of helium is believed to be caused by the appearance of quasars at lower redshifts and is therefore included in CAMB by a second step at $z = 3.5$, see figure 2.

An alternative parametrization of reionization has recently been proposed in [39]. Based on Lyman- α emission of star forming galaxies and Gunn-Peterson optical depths of quasars

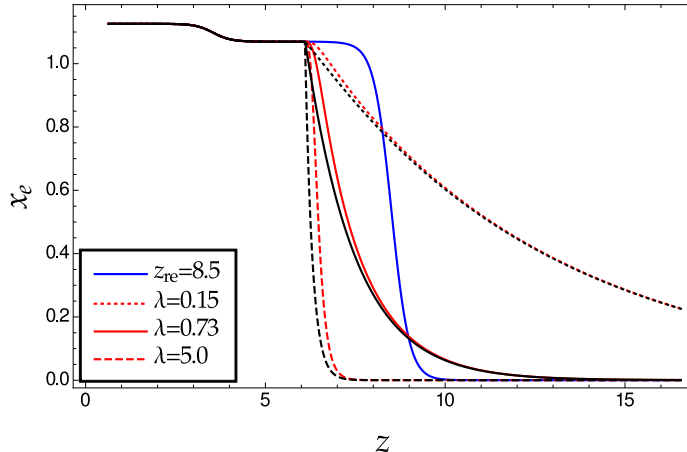


Figure 2: The free electron fraction during the epoch of reionization. The CAMB parametrization (2.1) (blue line) is compared to the empirical parametrization (2.5) (red lines). The black lines describe the sharp edge introduced in (2.4), whereas the red curves show a smoothed version used in this work, see appendix A for details.

[40], the authors propose the following asymptotic behaviour of the ionised hydrogen fraction $Q_{\text{HII}} = n_{\text{HII}}/n_{\text{H}}$

$$\begin{aligned} 1 - Q_{\text{HII}} &\propto (1+z)^3 && \text{for } z < z_{\text{p}} \\ Q_{\text{HII}} &\propto \exp(-\lambda(1+z)) && \text{for } z \geq z_{\text{p}}. \end{aligned} \quad (2.3)$$

Such an empirical parametrization is also corroborated by numerical simulations that show extended scenarios of reionization [41, 42]. As proposed in [39], this parametrization can be characterized by three free parameters: the pivot redshift z_{p} , the ionised hydrogen fraction at the pivot scale $Q_{\text{p}} = Q_{\text{HII}}(z_{\text{p}})$ and the evolution parameter in the exponential λ . This translates into the following parametrization of Q_{HII}

$$Q_{\text{HII}}(z) = \begin{cases} \frac{1-Q_{\text{p}}}{(1+z_{\text{p}})^3-1} ((1+z_{\text{p}})^3 - (1+z)^3) + Q_{\text{p}} & \text{for } z < z_{\text{p}} \\ Q_{\text{p}} e^{-\lambda(z-z_{\text{p}})} & \text{for } z \geq z_{\text{p}}. \end{cases} \quad (2.4)$$

We furthermore assume that $Q_{\text{HII}}(z=0) = 1$, in order to fix the last degree of freedom that is allowed by (2.3). According to [39] the best-fit parameters are: $z_{\text{p}} = 6.1$, $Q_{\text{p}} = 0.99986$ and $\lambda = 0.73$. Note that these fits are based on *direct observations* of Q_{HII} .

In order to compare this parametrization to the one used by CAMB, (2.1), we first have to find an expression for the free electron fraction x_{e} , as defined in (2.2). Since Q_{HII} only accounts for the first term in eq. (2.2), we have to make an additional assumption about the ionization of helium. Considering the relatively similar ionization energies of 13.6 eV for HI and 24.6 eV for HeI, it seems reasonable to assume that the first ionization of helium happens in the same manner as the ionization of hydrogen. In that case, we can simply write

$$x_{\text{e}}(z)|_{\text{emp.}} = 1.08 \times Q_{\text{HII}}(z) \quad (2.5)$$

and the second ionization is described by a second step at $z = 3.5$, analogously as in the CAMB parametrization (2.1), see figure 2.

For $z < z_{\text{p}}$, Q_{HII} is tightly constrained by astrophysical observations [40]. Therefore, in the following we fix Q_{p} and z_{p} to the best-fit values quoted above, and keep λ as the single

free parameter. We refer to the parametrization (2.5) as *empirical parametrization* and to (2.1) as *CAMB parametrization* in the rest of this work.

In figures 1 and 2 we show the free electron fraction as a function of redshift for the empirical parametrization (2.5) for three different values of λ compared to the CAMB parametrization (2.1) with $z_{\text{reio}} = 8.5$. The empirical parametrization with small values of λ allows for more extended reionization histories than the CAMB parametrization with $\Delta_z = 0.5$.

Equation (2.4) exhibits a sharp edge at $z_p = 6.1$ and therefore leads to a discontinuity in the derivatives of the visibility function. We therefore have to smooth x_e (2.5) at z_p in order to remove unphysical bias. Details can be found in the appendix A. We include a plot of the smoothed version of eq. (2.4) in figure 2.

2.2 Impact of astrophysical reionization on CMB angular power spectra

Reionization affects the high- ℓ and low- ℓ CMB spectra in two ways:

- i) The CMB temperature fluctuations experience a suppression of $e^{-\tau}$, where τ denotes the optical depth defined as

$$\tau(z) \equiv c \int_z^0 n_e(z') \sigma_T \frac{dt}{dz'} dz'. \quad (2.6)$$

Above t denotes cosmic time and σ_T is the Thomson scattering cross section. The temperature angular power spectrum (TT) is therefore suppressed by a factor of $e^{-2\tau}$. Thus the optical depth τ is degenerate with the amplitude of primordial curvature fluctuations, described by A_s (we do not consider primordial tensorial fluctuations in this work). The suppression is present at all scales that are subhorizon before recombination, i.e. $\ell \gtrsim 200$. For lower ℓ the suppression of the spectrum is less pronounced, as these modes enter the horizon after recombination or even after reionization ($\ell \lesssim 20$).

- ii) The polarization angular power spectra (parity-even E-modes and parity odd B-modes, the latter are not further studied in this work) reflect the size of the temperature quadrupole at the time of last scattering at a given scale. The polarization and cross angular power spectra (TE, TB, EE, EB, BB) are also suppressed by a factor $e^{-2\tau}$. But more importantly, reionization also causes polarization at large scales, where without reionization there would be no polarization source due to the lack of electrons that could scatter the intensity quadrupole. This effect shows up as a bump in the polarization angular power spectra at low ℓ and is a unique feature of reionization as it can only be caused by a late time effect.

Therefore, the high- ℓ TT and EE spectra only depend on the amount of reionization, but not on the details of the reionization history itself. There are however two important caveats to this simplistic picture: Firstly and most importantly for the scenarios considered in this work, the low- ℓ data have in principle the potential to distinguish between different reionization histories. This can be seen in figure 3, where we show the low- ℓ EE spectrum for the CAMB reionization (2.1) and the empirical reionization (2.5) for the same values of the optical depth. The CAMB parametrization gives rise to more polarization power at low ℓ than the empirical parametrization. This difference is more pronounced for high values of τ and vanishes for small τ . It is also important to ask how the difference between reionization histories compares to cosmic variance of the polarization power spectra. This is shown in the

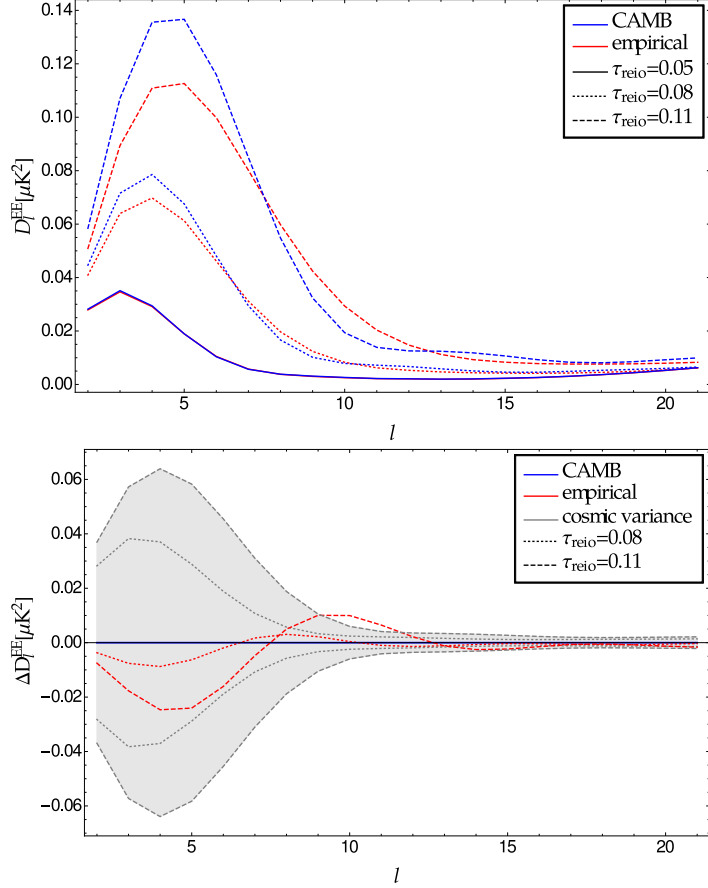


Figure 3: Top panel: Comparison of the CMB EE angular band power spectra ($D_\ell^{EE} = \ell(2\ell + 1)C_\ell^{EE}/2\pi$) for the CAMB (2.1) (blue lines) and empirical parametrizations (2.5) (red lines) for three different values of the optical depth. Bottom panel: Difference $\Delta D_\ell^{EE} = D_{\ell,\text{emp}}^{EE} - D_{\ell,\text{CAMB}}^{EE}$ in the EE spectrum (red lines) at equal optical depth. The shaded regions represent the cosmic variance for the respective values of the optical depth.

lower figure 3. We notice that the differences are less significant at very small ℓ , but can be larger than the cosmic variance for individual multipole moments at $\ell \sim 10$ and above. See also [43], [19] or [23] for other examples of different reionization histories and their impact in the low- ℓ polarization spectrum.

Secondly, as shown in [21, 23], for significant changes in the reionization history at *early* times, the suppression of the high- ℓ CMB spectra becomes oscillatory and the simple picture described above breaks down. This effect stems from substantial changes in the visibility function at early times, but turns out to be irrelevant for all scenarios considered in this work.

In figure 4, we show the CMB TT, EE and TE angular power spectra for the CAMB parametrization (2.1) with the Planck 2015 best-fit value $z_{\text{re}} = 8.5$ ($\tau_{\text{reio}}=0.061$) [24] and the empirical parametrization (2.5) for the best-fit value $\lambda = 0.73$ ($\tau_{\text{reio}}=0.053$) [39]. The figure also includes the effect of DM decay which we discuss later in section 3.4.

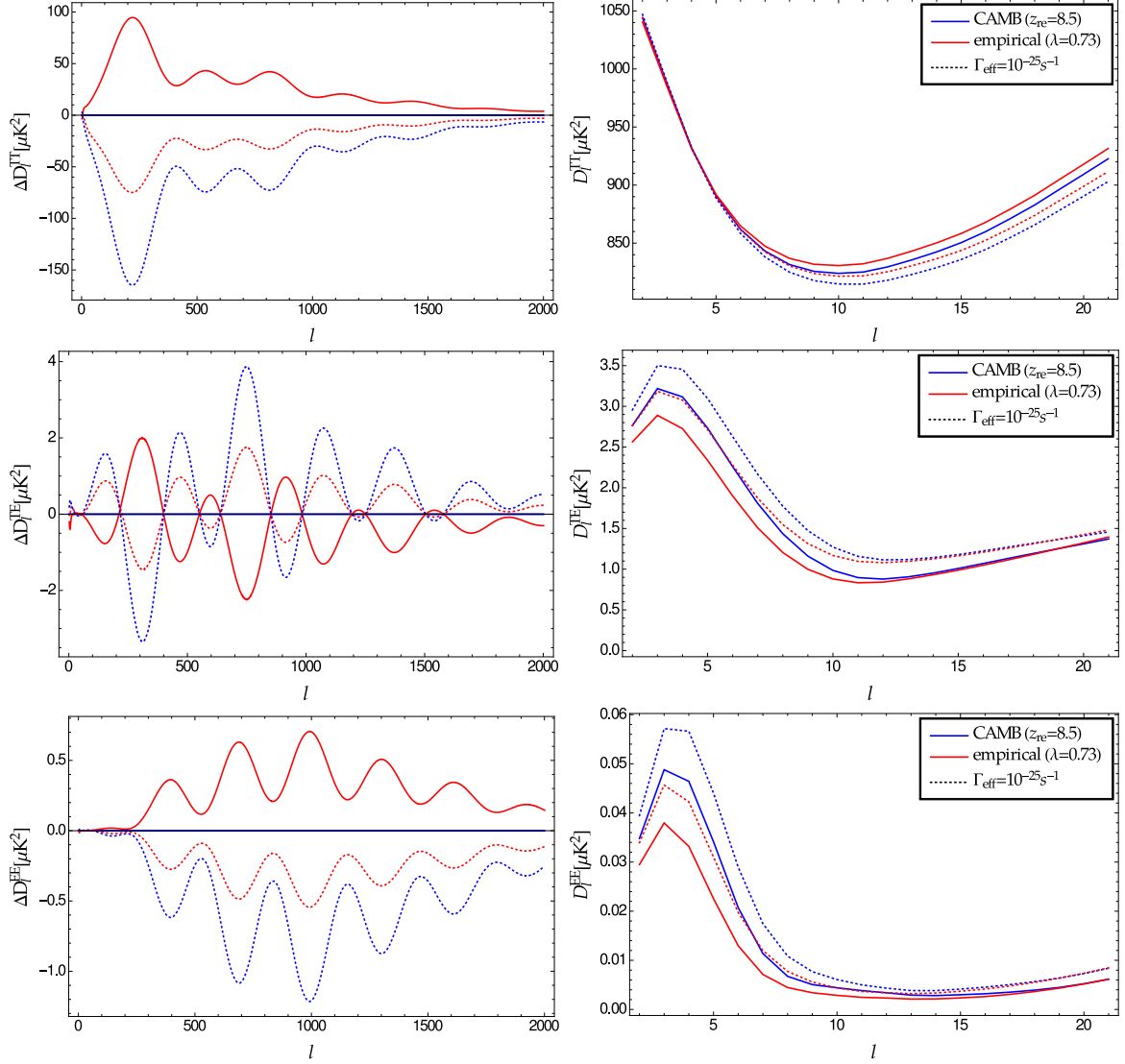


Figure 4: CMB angular band power spectra (top row: TT, middle row: TE, bottom row: EE) for the CAMB parametrization (2.1) with $z_{\text{re}} = 8.5$ (blue lines), the empirical parametrization (2.5) with $\lambda = 0.73$ (red lines), both with (dashed lines) and without (solid lines) dark matter decay for $\Gamma_{\text{eff}} = 10^{-25} \text{s}^{-1}$. The left column shows the angular band power difference to the CAMB parametrization ($z_{\text{re}} = 8.5$) without dark matter decay, $\Delta D_\ell = D_{\ell,i} - D_{\ell,\text{CAMB}}$. The right column shows the band spectra in the so-called reionization bump region at low multipole moments $\ell < 20$.

3 Dark matter decay and cosmic reionization

3.1 Dark matter decay

Let us turn to study the impact of an additional source of reionization, namely the decay of dark matter. To avoid any source of confusion, we will refer to the late time reionization by astrophysical objects, i.e. (2.1) or (2.5), by *astrophysical reionization* and to reionization due to DM decay or annihilation by *DM reionization*.

Various works investigated such scenarios of DM reionization, e.g. [18–22, 25–29], most of them focussing on DM annihilations. But all of these studies are based on the CAMB parametrization of astrophysical reionization (2.1). Only recently, the authors of [23] have investigated the impact of DM halo formation on the reionization history, considering thereby for the first time *two different astrophysical reionization histories*. They came to the conclusion that in the case of the CAMB parametrization (2.1), the influence of halo formation is negligible, whereas for an alternative parametrization based on the star formation rate, the impact of halo formation can become substantial. This immediately calls for a closer investigation of the impact of our assumptions about astrophysical reionization on constraints of DM properties. In the following, we start with a description of the impact of DM decay to the reionization history.

The evolution of the number density n_d of the decaying DM particles is described by the equation of radioactive decay in an expanding universe,

$$\dot{n}_d(t) + 3Hn_d(t) = -\Gamma_{\text{tot}}n_d(t). \quad (3.1)$$

Here $\Gamma_{\text{tot}} = \Gamma_{\text{em,s}} + \Gamma_{\text{w}}$ is the sum of the decay rate into particles only interacting via weak force (neutrinos), Γ_{w} , and the decay rate into particles interacting via electromagnetic and/or strong force, $\Gamma_{\text{em,s}}$. We refer to this decaying particle as DM, even though we do not restrict to the case where it constitutes all DM in the universe. The solution of equation (3.1) is given by

$$n_d = n_{d,i} \left(\frac{a_i}{a}\right)^3 e^{-\Gamma_{\text{tot}}(t-t_i)} = n_{d,i} \left(\frac{1+z}{1+z_i}\right)^3 \exp\left(-\Gamma_{\text{tot}} \int_z^{z_i} \frac{dz}{(1+z)H(z)}\right), \quad (3.2)$$

where $n_{d,i}$ is the initial number density. For low decay rates Γ_{tot} or at sufficiently early times t , we find $n_d \propto a^{-3}$, i.e. the dominant dilution effect is due to the expansion of the universe.

3.2 Energy deposition from dark matter decay

The decaying DM injects energy into the cosmic hydrogen-helium gas. The energy that is injected per time and volume via electromagnetically or strongly interacting particles into the medium by the decay is given by

$$\left(\frac{dE}{dt dV}\right)_{\text{inj}} = \Delta E_d \Gamma_{\text{em,s}} n_d(t). \quad (3.3)$$

To indicate that we also include the scenario for a DM particle going from an excited to some lower state, we have written ΔE_d in (3.3). In such a scenario, n_d also has to be interpreted as the number density of the excited state. For the case of DM decay into standard model particles, we have $\Delta E_d = m_d$, where m_d is the DM mass.

In general, not all of the injected energy is immediately deposited into the surrounding medium. If the density of the neighbouring gas is low, the emitted particles experience redshift before they are absorbed. This effect depends on the redshift of consideration, on the injected energy ΔE_d as well as the nature of the emitted particles. The total effect is usually very hard to compute, because it includes the formation of cascades and their efficiency to ionize the gas. Moreover, decay products in the form of neutrinos lead to further energy loss, because neutrinos simply free-stream and do not interact with the medium. In general, the relation between injected and emitted energy is given by

$$\left(\frac{dE}{dt dV}\right)_{\text{dep}}(z) = \int_z^\infty F_m(z, z_{\text{inj}}, \Delta E_d) \left(\frac{dE}{dt dV}\right)_{\text{inj}}(z_{\text{inj}}) dz_{\text{inj}}, \quad (3.4)$$

where the function $F_m(z, z_{\text{inj}}, \Delta E_d)$ describes the fraction of the energy injected at redshift z_{inj} which is deposited at redshift z . The label m indicates the dependence on the specific model of DM decay. However, it is a common practice to include this effect by a function $f_m(z, \Delta E_d)$ that encapsulates the above integral, which in combination with eq. (3.3) gives

$$\begin{aligned}
\left[\frac{dE}{dt dV} \right]_{\text{dep}}(z) &= \left[\frac{1}{\left[\frac{dE}{dt dV} \right]_{\text{inj}}(z)} \int_z^\infty F_m(z, z_{\text{inj}}, \Delta E_d) \left[\frac{dE}{dt dV} \right]_{\text{inj}}(z_{\text{inj}}) dz_{\text{inj}} \right] \left[\frac{dE}{dt dV} \right]_{\text{inj}}(z) \\
&\equiv f_m(z, \Delta E_d) \left(\frac{dE}{dt dV} \right)_{\text{inj}}(z) \\
&= \frac{m_p}{0.76} n_H(z) f_m(z, \Delta E_d) \left(\frac{\Delta E_d}{m_d} \right) \left(\frac{\rho_d}{\rho_b} \right) \Gamma_{\text{em},s} \\
&= 1.23 \times 10^9 n_H(z) f_m(z, \Delta E_d) \left(\frac{\Delta E_d}{m_d} \right) \left(\frac{\rho_d}{\rho_b} \right) \Gamma_{\text{em},s} \text{ eV}, \tag{3.5}
\end{aligned}$$

where n_H is the number density of hydrogen and we use $n_H = 0.76 n_b$ in the second line.

From now on we focus on cases where $(\rho_d/\rho_b) \simeq \text{const}$, i.e. lifetimes much larger than the age of the universe or $\Gamma_{\text{tot}} \lesssim 10^{-17} \text{ s}^{-1}$. Inclusion of higher decay rates would furthermore demand the modification of the Friedmann equations to take into account the decay of non-relativistic matter into radiation [44–46]. If the decaying particle makes up all dark matter of the universe we have $(\rho_d/\rho_b) \approx 5.5$, but we keep the possibility of $0 < (\rho_d/\rho_b) \lesssim 5.5$. Since eq. (3.5) depends in the same way on (ρ_d/ρ_b) , $(\Delta E_d/m_d)$ and $\Gamma_{\text{em},s}$, it is convenient to summarize these three parameters as

$$\Gamma_{\text{eff}} = \left(\frac{\Delta E_d}{m_d} \right) \left(\frac{\rho_d}{\rho_b} \right) \Gamma_{\text{em},s} \tag{3.6}$$

and therefore

$$\left(\frac{dE}{dt dV} \right)_{\text{dep}} = 1.23 \times 10^9 n_H f_m(z, \Delta E_d) \Gamma_{\text{eff}} \text{ eV}. \tag{3.7}$$

3.2.1 On-the-spot approximation

The function $f_m(z, \Delta E_d)$ can for example be computed for different ΔE_d with the publicly available code described in [47]. Taking into account the full possible energy range of ΔE_d into a cosmological data analysis is in general computationally expensive. In section 4.2 our aim is in the first place to investigate how much these constraints depend on our assumptions about astrophysical reionization. Therefore we restrict our analysis here to an energy range that allows us to use the so called *on-the-spot* approximation in which $f_m(z, \Delta E_d) = 1$. This approximation restricts the validity of our analysis to $\Delta E_d \lesssim 1 \text{ keV}$ [47, 48].

In section 4.4, we apply our work to warm DM candidates such as keV-mass sterile neutrinos [34]. The specific parameters for this DM candidate can be constrained via a reinterpretation of the constraints on Γ_{eff} , as is shown in section 4.4. Additionally to the on-the-spot approximation, we also consider the full redshift range of $f_m(z, \Delta E_d)$ by using a fitting formula of the deposition efficiency obtained by [49].

3.3 Reionization from dark matter decay

To find the evolution of the free electron function x_e we have modified the recombination code CosmoRec and included the new energy source term described in eq. (3.5). As a further

input we need to include how the energy (3.5) is distributed, i.e. how much energy goes into ionization and excitation of atoms and how much into heating of the medium. The CosmoRec code already contains a module for DM annihilation and we assume that the DM decay has the same energy distribution, as described in [20, 50]. As usual, the output of CosmoRec is included in the Boltzmann solver CAMB and then at some lower redshift the CAMB reionization module initiates the astrophysical reionization, i.e. (2.1) or (2.5).

We use the Recfast++ module of CosmoRec to model the effect of DM decay on the ionization history. This allows us to capture the main recombination physics corrections around $z \sim 1000$ (e.g., [51]), while providing sufficient flexibility to account for large energy injection.

There are two further effects that need to be taken into account, as described in detail in [52] for the case of heating by primordial magnetic fields:

- i) The photon ionization coefficient has to be evaluated as a function of photon temperature T_γ , not electron temperature T_e . Negligence of this can lead to a strong overestimation of the photon ionization rate which results in an extremely sudden increase of the free electron fraction.
- ii) Collisional ionization effects become efficient for $T_e \gtrsim 10^4 \text{K}$ and therefore should be included in Recfast++. Large decay rates Γ_{eff} lead to an enhancement of the ionization rate and hence to an increase of the free electron fraction.

Both corrections are negligible for astrophysical recombination histories, but are very important for DM decay. In figure 5, we show the impact of these corrections on the free electron fraction x_e and the electron temperature T_e for $\Gamma_{\text{eff}} = 10^{-25} \text{ s}^{-1}$ and $\Gamma_{\text{eff}} = 10^{-24} \text{ s}^{-1}$. Note that both plots only show the output of CosmoRec (in Recfast++ mode). The astrophysical reionization by CAMB, eq. (2.1) or (2.5), is *not* yet added. Without both corrections (dotted line), the free electron fraction shows a very abrupt and implausible increase at $x_e \sim 0.05$. For both displayed Γ_{eff} this unphysical transition happens at $z \geq 6$, i.e. possibly before the onset of astrophysical reionization, and leads to a serious overestimation of the impact of DM decay on the free electron fraction. We believe that earlier investigations, e.g. [22, 29], have overlooked this effect. When correction i) is taken into account (dashed line), the sudden transition disappears and the function becomes smoother. Correction ii), the impact of collisional ionizations (solid line), is significant at $z \gtrsim 6$ for $\Gamma_{\text{eff}} = 10^{-24} \text{ s}^{-1}$, but not for $\Gamma_{\text{eff}} = 10^{-25} \text{ s}^{-1}$. When the electron temperature reaches $\sim 10^4 \text{ K}$, collisional ionizations become efficient, leading to a cooling of T_e and an enhancement of x_e . As soon as all atoms are ionized, the electron temperature starts to increase again.

In figure 6 we show the evolution of the free electron fraction for different values of Γ_{eff} and for both scenarios of the astrophysical reionization. To obtain a smooth transition from CosmoRec to CAMB we add up the contributions from both codes as described in the appendix A. Note that with this procedure the interpretation of the evolution parameter λ is different from the case without DM decay: For pure astrophysical reionization, λ is a parameter that can directly be observed from astrophysical data. But when including DM decay the evolution of the free electron fraction is effectively described by astrophysical reionization and DM decay, the direct observation is hence a combination of λ and Γ_{eff} . In this case λ has to be interpreted as a parameter describing the astrophysical reionization process and not as a parameter describing direct observations.

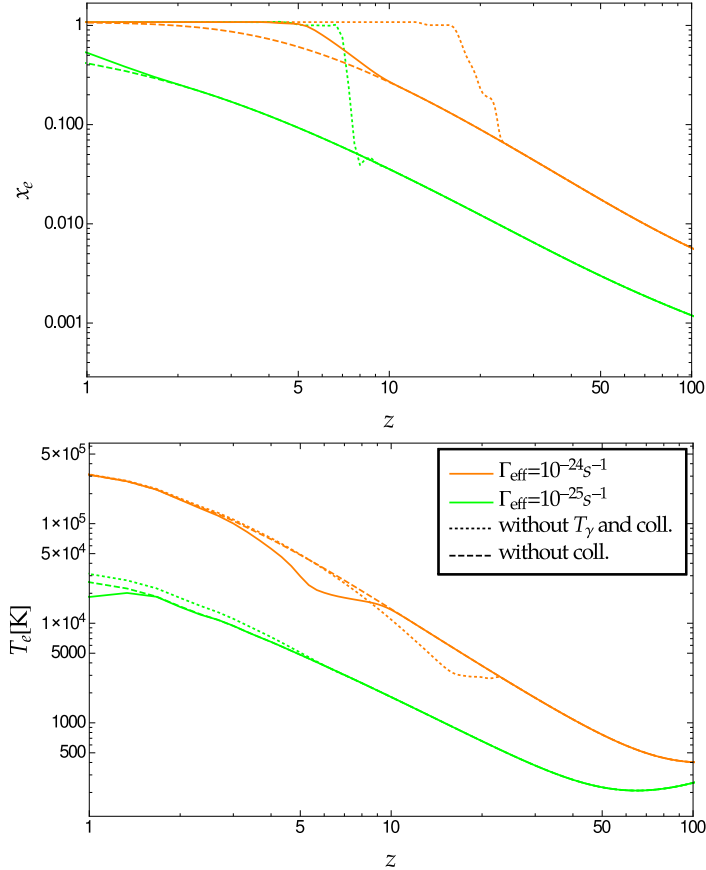


Figure 5: Cosmic reionization from dark matter decay. We plot the evolution of the free electron fraction (top panel) and the electron temperature (bottom panel) for $\Gamma_{\text{eff}} = 10^{-25} \text{ s}^{-1}$ (green lines) and $\Gamma_{\text{eff}} = 10^{-24} \text{ s}^{-1}$ (orange lines), ignoring contributions from astrophysical reionization. Dotted lines: The output produced by the public Recfast++ run mode. Dashed lines: First code modification to evaluating the photon ionization coefficient at the photon temperature T_γ . Solid lines: Second code modification to include collisional ionizations.

3.4 Impact of dark matter decay on CMB angular power spectra

In figure (4), we show the TT, EE and TE angular power spectra for the CAMB parametrization (2.1) and the empirical parametrization (2.5) of astrophysical reionization with and without DM decay, where we use Planck best fit values of the parameters [24].

The impact of DM decay on the TT and high- ℓ EE angular power spectrum can roughly be understood in the same manner as the impact of astrophysical reionization described in section 2.2. Therefore, the differences at large ℓ that we see in this figure can be traced back to different values of the optical depth for the four considered τ models. The polarization spectrum at low ℓ in contrast does not only depend on the size of τ , but also on the evolution of the free electron fraction. As expected, we observe that DM decay leads to an enhancement in the EE and TE spectra at intermediate and low ℓ . We see that there are clear differences between the models for stable and unstable dark matter for all three spectra. Very extended reionization scenarios like DM decay lead to an enhancement of the polarization power at higher ℓ than rather sharp scenarios like astrophysical reionization. The importance of low- ℓ

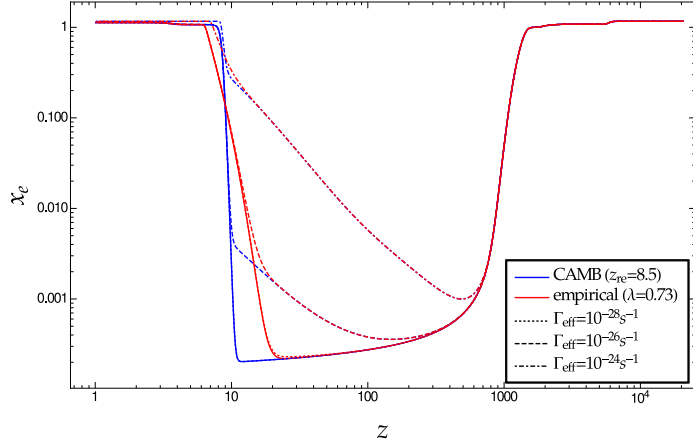


Figure 6: Effect of dark matter decay on the evolution of the free electron fraction. Solid lines are for stable DM, while broken lines show the effect of DM decay for $\Gamma_{\text{eff}} = 10^{-28}\text{s}^{-1}$ (dotted), $\Gamma_{\text{eff}} = 10^{-26}\text{s}^{-1}$ (dashed) and $\Gamma_{\text{eff}} = 10^{-24}\text{s}^{-1}$ (dash-dotted). The blue lines show the results for the CAMB parametrization (2.1) with $z_{\text{re}} = 8.5$, the red lines for the empirical parametrization (2.5) (red lines) with $\lambda = 0.73$.

$\Omega_b h^2$	$\Omega_c h^2$	θ_s [deg]	$\ln(10^{10} A_s)$	n_s
0.02226	0.1193	1.04087	2.0 – 4.0	0.8 – 1.2

Table 1: Cosmological parameters of the flat Λ cold dark matter models in our Markov chain Monte Carlo (MCMC) analysis. The dimensionless baryon and cold dark matter densities and the angular size of the acoustic sound horizon are fixed to their best-fit values from the Planck 2015 analysis. For the primordial scalar amplitude and the spectral tilt we indicate the range of the the flat prior distribution.

polarization data to constrain the DM decay rate Γ_{eff} becomes evident.

4 Constraints from CMB observations

4.1 Model fitting and comparison

The objective of this analysis is to study the impact of our assumptions on astrophysical reionization on the inference of cosmological parameters. In section 4.2, we therefore compare the two different parametrizations introduced in section 2.1. We add DM decay as an additional source of reionization and derive constraints on the DM decay rate using both parametrizations of astrophysical reionization in section 4.3. This allows us to study the robustness of the constraints on the DM decay rate given the lack of information about astrophysical reionization. In section 10, we apply our analysis to a keV-mass sterile neutrino as a specific DM candidate and derive constraints on its mixing angle and mass.

We use the Bayesian approach to study the different reionization parametrizations with and without DM decay. In order to find the posterior distributions of cosmological parameters, we use a modified version of the publicly available Markov Chain Monte Carlo (MCMC)

CosmoMC run	z_{re}	λ	$-\log_{10}(\Gamma_{\text{eff}} \text{ s})$
CAMB parametrization	5.0 – 13.0	—	—
empirical parametrization	—	0.05 – 2.5	—
CAMB parametrization + DM decay	5.0 – 13.0	—	24 – 28
empirical parametrization + DM decay	—	0.05 – 2.5	24 – 28

Table 2: Range of flat priors for the reionization and dark matter decay parameters used in the MCMC analysis.

parameter estimation code CosmoMC [53]¹, which makes use of the Boltzmann solver code CAMB [54]². CAMB adopts the recombination history from a library produced by the CosmoRec code [37, 38]³. The modules of reionization (CAMB) and recombination (CosmoRec) were respectively modified to include the empirical parametrization (2.5) and the effect of DM decay, as described in sections 2 and 3.

The CosmoMC code treats the reionization optical depth τ_{reion} as a free parameter and derives the redshift of reionization z_{re} from it, using the parametrization (2.1). Since we investigate the empirical parametrization (2.5) within this work, treating τ_{reio} as a free parameter is impractical and we modified the code such that z_{re} (or λ in the empirical parametrization) is varied and we treat the optical depth as a derived parameter.

For the purpose of reionization analysis, it is not necessary to vary all six standard parameters of the flat Λ cold dark matter (Λ CDM) model. The dimensionless density of baryons ($\Omega_b h^2$), cold dark matter ($\Omega_c h^2$) and the angular diameter distance (θ_s) have very little or no degeneracy with the degrees of freedom related to reionization [24]. The reason is that these parameters affect the CMB spectrum (position and amplitude of peaks and wells) in a scale dependent way. Reionization takes place well after recombination and affects all high multipole moments in the same way. Similar overall effects can be caused by changing the initial power spectrum, therefore the parameters $\ln(10^{10} A_s)$ and n_s show a significant degeneracy with the parameters related to reionization and are kept free in this analysis.

The adopted values for the fixed parameters are kept to their best-fit values from the Planck 2015 analysis [24]. Table 1 shows those values as well as the prior ranges for the primordial power spectrum parameters of our analysis. Given our ignorance of the details of astrophysical reionization and the value of λ , we choose a flat prior in λ . Note that our choice of a flat prior for z_{re} means that the CAMB parametrization asks the question when does cosmic reionization happen, while a flat prior for λ for the empirical parametrization asks how fast does it happen, since in the empirical parametrization we know already the redshift z_p when most of the reionization is completed. This has important consequences for the results of our analysis, as we discuss in section 4.2. Table 2 describes the four MCMC runs with the respective adopted flat prior ranges of the parameters describing the different reionization parametrizations (z_{re} and λ) and the decay of DM (Γ_{eff}).

For the inference procedure, we use the Planck 2015 data [24] including three likelihoods: (i) the low- l temperature and LFI polarization (bflike, $2 \leq \ell \leq 29$), (ii) the high- l plik TTTEEE ($30 \leq \ell \leq 2508$) likelihood, and finally (iii) the lensing power spectrum reconstruction likelihood. Throughout this paper, this data set is called “Planck lowTEB & TT,

¹Version July 2015.

²Version January 2015.

³Version 2.0.3.

TE, EE & lensing”. The lensing reconstruction helps to fix the angular diameter distance and exempts the need for a low redshift measurement of standard markers such as baryonic acoustic oscillations or type Ia supernovae. This combination is among the data sets used in the reionization analysis contained in [24], which should facilitate the comparison. Planck 2016 intermediate data [55, 56] are not included, as they are not available for analysis yet.

We adopt the Gelamann-Rubin convergence criterion (variance of chain means divided by the mean of the chain variances) of $R - 1 < 0.05$.

4.2 Comparison of astrophysical reionization models

In figure 7 we show the 68% and 95% confidence levels of $\ln(10^{10} A_s)$, n_s along with the empirical parametrization (λ) as well as the CAMB parametrization (z_{re}). The corresponding mean averages and lower limits are listed in table 3.

We observe that models with $\lambda < 0.37$ are excluded at 95% confidence level which roughly translates into $\tau_{\text{reio}} \lesssim 0.07$. The CAMB parametrization in contrast shows $z_{\text{re}} < 10.3$, i.e. $\tau_{\text{reio}} \lesssim 0.08$. Very interestingly we furthermore find a significant enlargement of the posterior distribution of n_s comparing the empirical parametrization to the CAMB parametrization in figure 7.

The reason for these findings — tighter constraints on τ_{reio} and weaker constraints on n_s — lies within the different assumptions that we make when using the two different parametrizations of astrophysical reionization: The CAMB parametrization does not impose any prior knowledge about the redshift of reionization, but it makes assumptions about the process of reionization itself (i.e. more or less instantaneous reionization). The empirical parametrization in contrast (with fixed $Q_p = 0.99986$ and $z_p = 6.1$) assumes some prior knowledge on the redshift of reionization, but allows for extended (small λ) as well as for sudden (large λ) reionization histories. Based on observations of quasars and star forming galaxies, the empirical parametrization assumes (almost) complete ionization for $z \leq 6.1$ and therefore has an intrinsic prior of $\tau_{\text{reion}} \gtrsim 0.04$.

The effect of implementing a prior of $\tau > 0.04$ in the CAMB parametrization is shown in figure 8. Also in that case we observe a spreading of the posterior of n_s . However, this effect alone would not explain why high values of the optical depth are disfavored for the empirical parametrization.

The preference of low values of the optical depth is in fact implied by our choice of a flat prior on the evolution parameter λ . A flat prior in z_{re} does in contrast lead to a relatively flat prior on the optical depth. We explain this in detail in appendix B. From the perspective of CMB data analysis, with τ_{reio} as a principal component of the CMB, one may argue that it is desirable to use a flat prior on τ_{reio} . However, from the perspective of reionization physics it appears more natural to us to assume a flat prior on λ , reflecting our ignorance of the evolution of the free electron fraction during reionization. The only thing we know about λ is its order of magnitude (best fit $\lambda = 0.73$ [39]) and we chose its flat prior range such that it covers the same range of τ_{reion} as is covered by the flat prior range of z_{re} . A similar discussion but on the use of priors for n_s and A_s in inflationary models can be found in [57].

Finally, the combination of both effects, i.e. the prior of $\tau_{\text{reion}} > 0.04$ (imposed by quasar and star forming galaxy observation) together with the preference of small values for τ_{reion} implied by a flat prior in λ , explains also the widening in the posterior of n_s . This is purely a normalization effect, as we show in more detail in appendix B. The interplay between n_s and τ depending on the assumed reionization history is one of our main results.

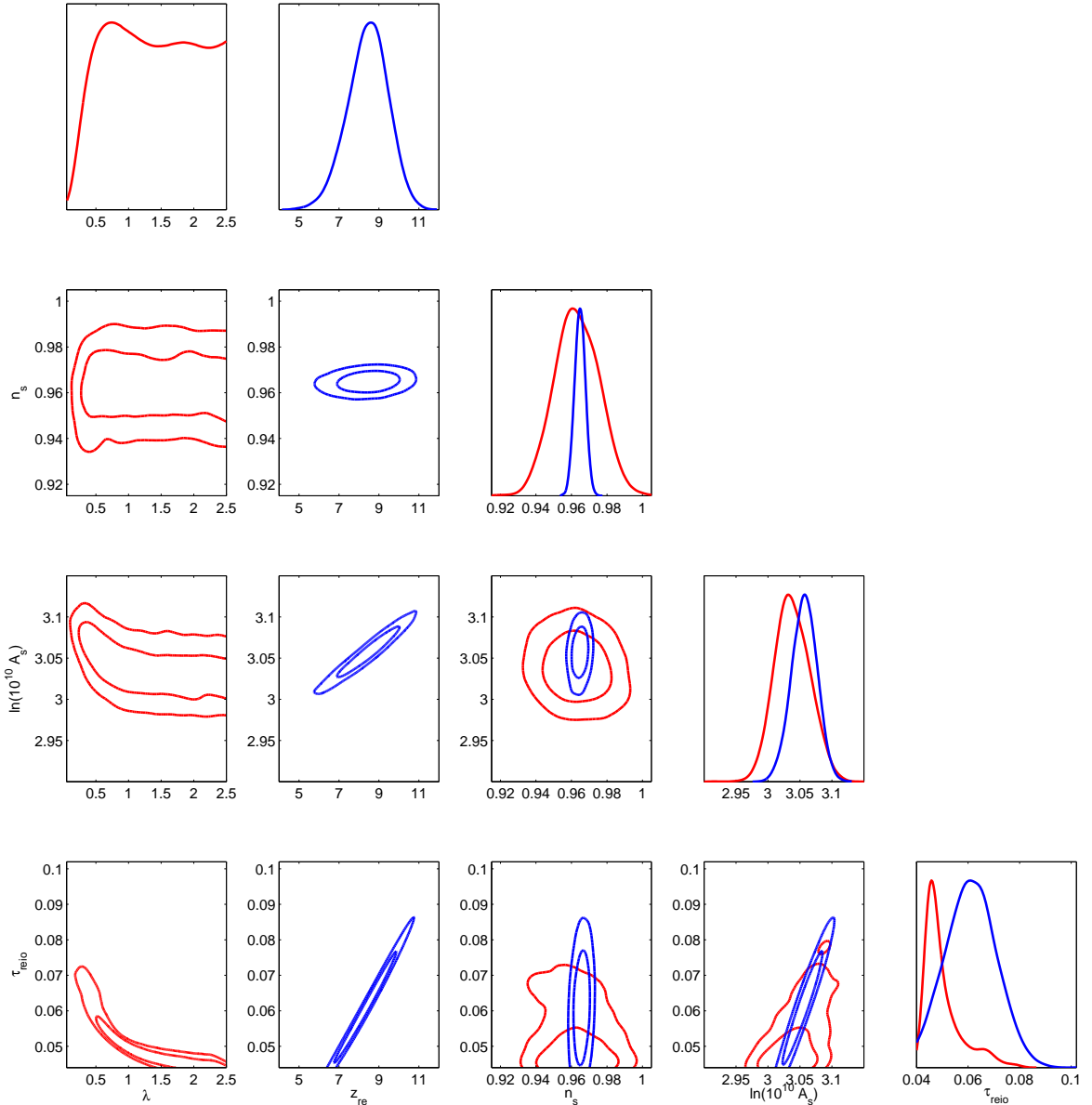


Figure 7: Model constraints for stable dark matter. 2d marginalized 68% and 95% confidence contours and 1d marginalized posterior distributions are shown for the free parameters constrained using Planck 2015 data (TT, TE, EE, lowTEB, lensing). The empirical parametrization (red lines, λ) and the CAMB parametrization (blue lines, z_{re}) are compared for a flat Λ CDM model.

4.3 Limits on dark matter decay rate

Let us now focus on the case of DM decay, see figure 9. We find $\Gamma_{\text{eff}} < 2.6 \times 10^{-25} \text{s}^{-1}$ for the CAMB parametrization and $\Gamma_{\text{eff}} < 2.9 \times 10^{-25} \text{s}^{-1}$ for the empirical parametrization. Since these constraints agree within $\sim 10\%$, we conclude that the constraints on DM properties show only a weak dependence on the chosen parametrization of reionization. This is reassuring, as it confirms that even though the details of astrophysical reionization are still widely

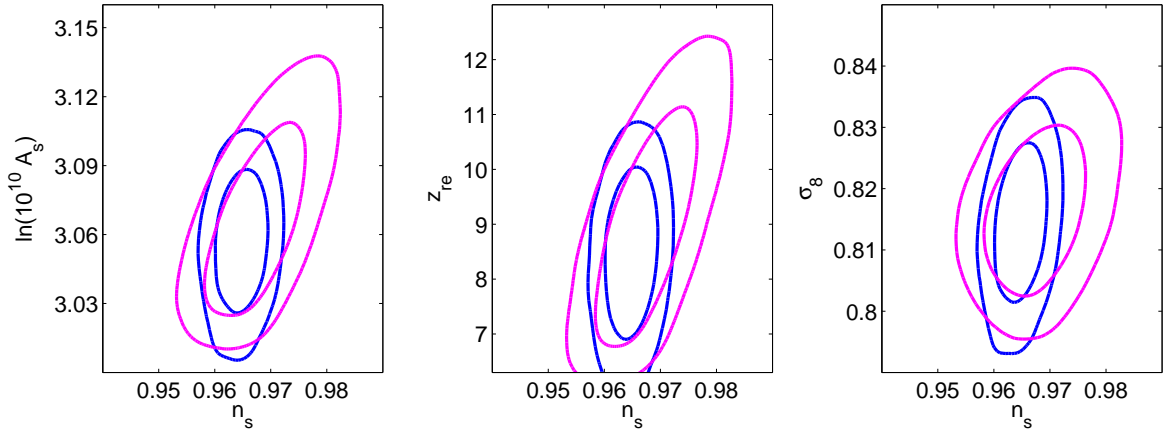


Figure 8: 2d marginalized constraints on cosmological parameters for stable dark matter. Blue lines: CAMB parametrization with the flat prior distribution for z_{re} from table 2. Magenta lines: CAMB parametrization with a flat prior on the optical depth and $\tau_{\text{reio}} > 0.04$.

CosmoMC run	$\ln(10^{10}A_s)$	n_s	z_{re}	λ	$-\log_{10}(\Gamma_{\text{eff}} \text{ s})$	$\Gamma_{\text{eff}} [s^{-1}]$
CAMB	$3.05^{+0.04}_{-0.03}$	$0.965^{+0.006}_{-0.007}$	$8.4^{+1.9}_{-2.0}$	—	—	—
empirical	$3.04^{+0.05}_{-0.05}$	$0.96^{+0.03}_{-0.02}$	—	> 0.37	—	—
CAMB & decay	$3.07^{+0.11}_{-0.09}$	$0.97^{+0.02}_{-0.03}$	$8.6^{+1.7}_{-3.1*}$	—	> 24.59	$< 2.6 \times 10^{-25}$
empirical & decay	$3.04^{+0.08}_{-0.06}$	$0.96^{+0.03}_{-0.02}$	—	$> 1.7*$	> 24.54	$< 2.9 \times 10^{-25}$

Table 3: Constraints on cosmological parameters based on Planck 2015 data (TT, TE, EE, lowTEB, lensing), for the CAMB and empirical parametrizations for astrophysical reionization along with the constraints on the decay rate of dark matter. We indicate the central value and the 95% confidence interval or the 95% lower or upper limits respectively. For the cases marked by an asterisk (*) the 68% interval or limit is quoted.

unknown the constraints on DM properties are nevertheless reliable. The robustness of the bounds can be explained by the following considerations: Early reionization, like DM decay, leads to an enhancement of the TE and EE spectra in the intermediate ℓ range ($\ell \approx 10 - 60$). In contrast, late astrophysical reionization enhances the spectra only at lower ℓ (see figure 4). For the same reason we also expect our limits on Γ_{eff} to be weaker if the TE+EE data were excluded, see [24] for a discussion about the dependence of the constraints on the DM annihilation rate on the TE+EE data.

Our limits on Γ_{eff} also rule out the scenario of pure DM reionization that is complete at $z_p = 6.1$. This can be seen as a positive evidence for an astrophysical reionization process.

It is also interesting to note that when including DM decay there is a remarkable enlargement of the n_s -likelihood for the CAMB parametrization compared to the case without DM decay (figure 7), whereas for the empirical parametrization it remains roughly the same. This can be explained by the fact that DM decay introduces extended reionization histories, a feature that cannot be mimicked by the CAMB parametrization alone but is to some extent already included in the empirical parametrization.

Note that our constraints refer to the effective DM decay rate Γ_{eff} (3.6). If we assume

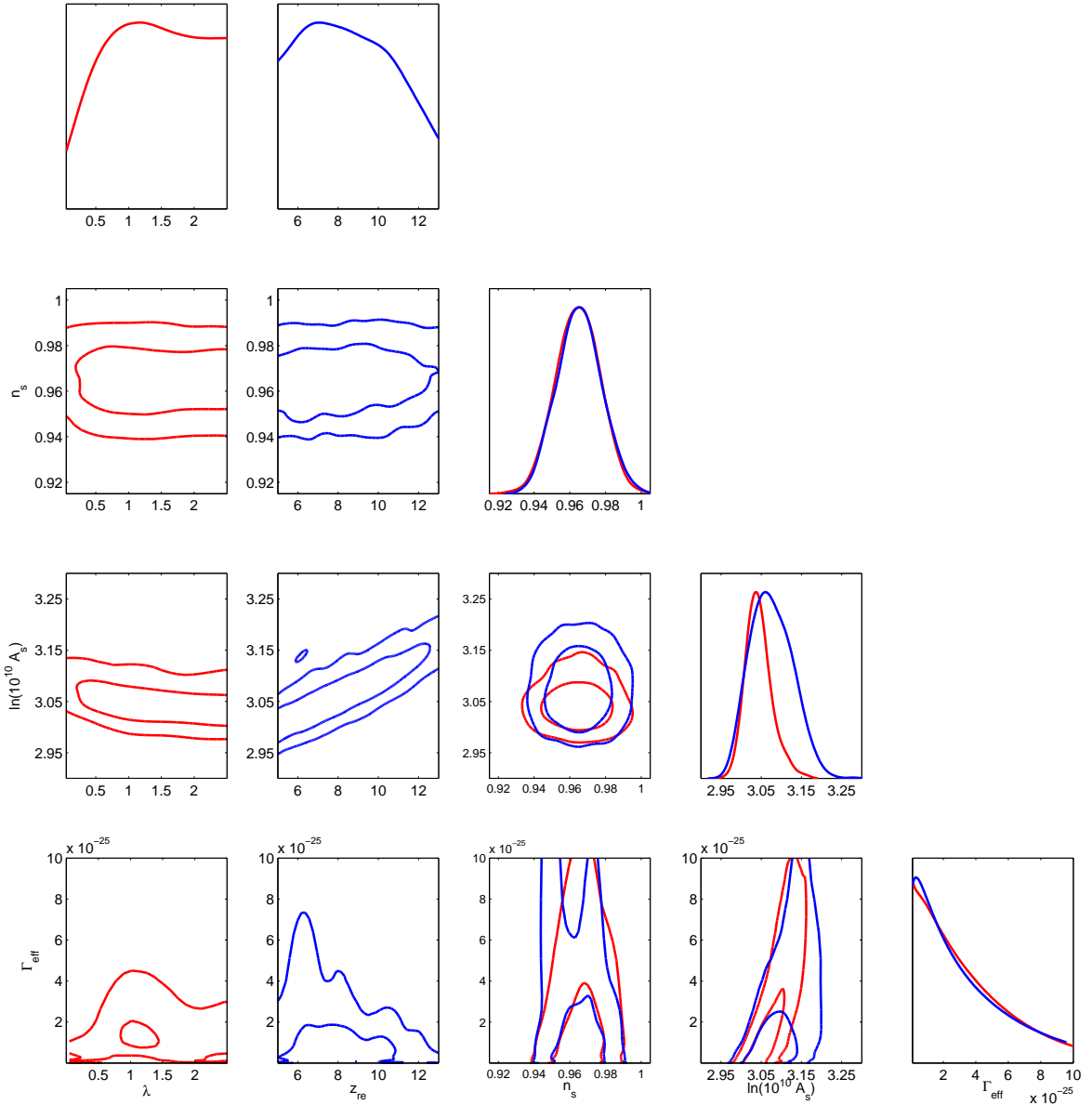


Figure 9: Model constraints for decaying dark matter. 2d marginal 68% and 95% confidence contours and 1d marginalized posterior distributions are shown for the free parameters constrained using Planck 2015 data (TT, TE, EE, lowTEB, lensing). The empirical parametrization (red lines, λ) and the CAMB parametrization (blue lines, z_{re}) are compared when the dark matter decay rate Γ_{eff} is added as an additional parameter.

that the decaying DM species makes up all DM of the universe, $(\rho_d/\rho_b) \approx 5.5$, the constraints on Γ_{eff} are translated into $\Gamma \lesssim 5.3 \times 10^{-26} \text{s}^{-1}$ for the real DM decay rate. This constraint assumes that all of the mass of the decaying particle goes into electromagnetic components and contributes to the ionization at time scales well below a Hubble time.

We should also point out again that we work within the on-the-spot approach which assumes entirely efficient energy deposition, see section 3.2.1. Since this approximation in general holds only for high redshifts, the constraints presented in this section are overesti-

mated and have to be treated with care. It is a common practice, e.g. [24, 29], to go beyond the on-the-spot approximation by including a DM mass dependent constant instead of taking into account the full redshift dependence of $f_m(z, \Delta E_d)$. This kind of effective treatment can also be applied to our constraints on Γ_{eff} , the prefactor that depends on the specific DM model can be calculated by codes like [47].

In the next section however, we consider the keV-mass sterile neutrino as a specific DM candidate, derive constraints on its decay rate and thereby go beyond the on-the-spot approximation.

4.4 Constraints on sterile neutrino dark matter

An interesting candidate for decaying DM is the sterile neutrino with masses of the order of keV. Several production mechanisms for sterile neutrino DM have been proposed (see [34] for a review). From the constraints on the decay rate of dark matter, we derive model independent constraints on sterile neutrino parameters. In order to compare our bounds with existing limits (some of them model dependent), we illustrate these constraints in the context of the already ruled out non-resonant freeze-in production of sterile neutrino (Dodelson-Widrow model) [58]. We also assume that sterile neutrinos are the only form of DM.

According to the Dodelson-Widrow model, sterile neutrinos are produced via non-resonant chiral oscillations of the left-handed neutrinos, forming a warm⁴ component of DM, which manifests itself as a strong suppression of structure below the free streaming length of sterile neutrinos. This suppression can be used to impose lower limits on the sterile neutrino mass by measuring structures at very small scales, using e.g. surveys of Lyman- α forest or kinetic equilibrium of dwarf galaxies.

Sterile neutrinos at this mass scale also have a radiative decay channel ($\nu_s \rightarrow \gamma + \nu_\alpha$), emitting an active neutrino and a photon, each with an energy equal to half of the sterile neutrino mass. The produced X-ray photon can be directly measured or, given its absence, can be used to impose upper limits on the decay rate. The decay rate $\Gamma_{\nu_s \rightarrow \gamma \nu_\alpha}$ in turn is related to the sterile neutrino mass m_s and mixing angle with active neutrinos θ in the following way

$$\Gamma_{\nu_s \rightarrow \gamma \nu_\alpha} = \frac{9\alpha G_F^2}{256 \times 4\pi^4} \sin(2\theta)^2 m_s^5, \quad (4.1)$$

where α is the fine structure constant and G_F the Fermi constant. A complete and comprehensive review on keV sterile neutrino DM can be found in [34].

Alternatively to direct observations, we can use the effect that the emitted X-rays would have on reionization. We derive constraints on the sterile neutrino decay rate $\Gamma_{\nu_s \rightarrow \gamma \nu_\alpha}$ and reinterpret them in terms of the mass and the mixing angle of the sterile neutrino. As shown in the previous section 4.2, the constraints on Γ_{eff} are independent of the chosen parametrization of astrophysical reionization. Hence we consider in this part of our analysis the empirical parametrization only, since it gives the most conservative constraint on the decay rate.

In order to model the effect of keV sterile neutrino decay on reionization in a realistic way, we have to go beyond the on-the-spot approximation which is only sufficient for deposited energies < 1 keV [48]. The function $f_m(z, \Delta E_d)$ that describes the energy deposition, see e.g. (3.7), can be evaluated numerically for each mass and redshift with the code of [47], but

⁴The notion of warm DM refers to the behaviour of the equation of state at the onset of structure formation, not to the question if they are thermal or non-thermal.

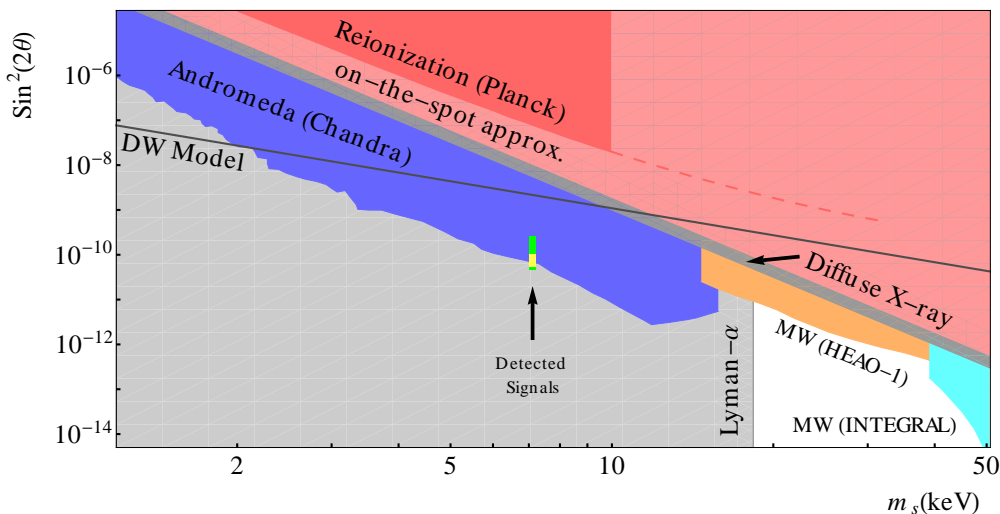


Figure 10: Illustration of reionization limits on decaying dark matter. We plot the parameter space of freeze-in keV sterile neutrino dark matter. The light red area labelled “on-the-spot approx.” is excluded by the decay rate constraint $\Gamma_{\text{eff}} < 2.9 \times 10^{-25}/\text{s}$ obtained in section 4.2. The dark red area takes corrections to the on-the-spot approximation [49] into account, valid for $2 \leq m_s/\text{keV} \leq 10$. The dashed red line extrapolates the latter constraint to $m_s > 10$ keV. Other regions of parameter space are excluded by the Tremaine-Gunn condition on the kinetic stability of dwarf galaxies ($m_s < 0.5$ keV is excluded) [59], the diffuse X-ray background [60], the observed flux of X-rays from Andromeda [61] and the Milk Way [62, 63], and a Lyman- α limit on the suppression of small scale structure for non-resonant production based on the bounds from [64] and the conversion formula from [65]. The latter limit is only valid for the Dodelson-Widrow (DW) non-resonant freeze-in model [58], which is depicted by the black line. For other models of sterile neutrino production, the Lyman- α limit depends not only on m_s but also on θ [66]. The claimed evidence for keV sterile neutrinos is shown in yellow [35] and green [36].

for our purpose it is much more convenient to use the fitting formula derived in [49],

$$f_m(z, \Delta E_d) = \left[0.5 + 0.032 \left(\frac{m_s}{8\text{keV}} \right)^{1.5} \right] \left[\frac{z}{110 \left(\frac{m_s}{8\text{keV}} \right)^{2.4} + z} \right]^{0.93}. \quad (4.2)$$

This formula is valid for masses $2 \leq m_s/\text{keV} \leq 10$. Including function (4.2) results in a reduction of the free electron fraction compared to the on-the-spot approximation,⁵ where the reduction is more pronounced at low redshifts and high masses m_s .

We included eq. (4.2) into our implementation in CosmoRec and obtain mass dependent constraints on Γ_{eff} which can be described by the fitting formula

$$\Gamma_{\nu_s \rightarrow \gamma \nu_\alpha}(m_s) < 10^{-24} \left[1.29 + 2.11 \times 10^{-2} \left(\frac{m_s}{\text{keV}} \right) + 1.48 \times 10^{-2} \left(\frac{m_s}{\text{keV}} \right)^2 \right] \text{ s}^{-1}, \quad (4.3)$$

which is valid for $2 \leq m_s/\text{keV} \leq 10$.

⁵ $f_m(z, \Delta E_d) = \frac{1}{2}$ since half of the energy is lost in form of neutrinos.

The corresponding constraints on the mixing angle θ and the mass m_s are shown as the dark red area dubbed “Reionization (Planck)” in figure 10, whereas the light red area represents the constraints using the on-the-spot approximation ($\Gamma_{\nu_s \rightarrow \gamma \nu_\alpha} < 5.3 \times 10^{-26} \text{s}^{-1}$). The red dashed line is a polynomial extrapolation (of 3rd order) of our results from $m_s \leq 10$ keV to higher masses in order to indicate the tendency of the constraint. The constraints derived from reionization are weaker than the constraints from the diffuse X-ray background [60]. However, they seem to be competitive and especially promising given the perspectives on the sensitivity to observe the reionization history by future surveys [67].

The model dependent cases of non-resonant oscillation [58], resonant production [66, 68] or decays of frozen-in scalars [69, 70] into sterile neutrinos would imply different abundances (lines in the $\theta - m_s$ plane) as well as different constraints from structure formation as the ones by the Lyman- α forest. A complete analysis that covers all possible models is beyond the scope of this work. The excluded Dodelson-Widrow non-resonant freeze-in model [58] is plotted as a benchmark solely. Nevertheless, the competitive constraint obtained on the decay rate using the effect on reionization can be easily mapped to different models.

A complementary study of sterile neutrinos and the reionization history can be found in [71], where the effect of free-streaming sterile neutrinos in the astrophysical reionization process itself was investigated.

5 Conclusions

In this work, we studied the impact of DM decay on the CMB considering two different parametrizations for astrophysical reionization – the conventional parametrization used by the CAMB code (2.1) (CAMB parametrization) and a recently proposed parametrization [39] based on astrophysical observations (2.5) (empirical parametrization). For equal values of the optical depth the empirical parametrization shows notable differences in the low- ℓ EE angular power spectrum of the CMB compared to the CAMB parametrization. Considering the decay of a DM species as an additional source of reionization, the CMB angular power spectra are furthermore sensitive to an effective DM decay rate Γ_{eff} (3.6). This effective decay rate includes not only the decay rate into electromagnetically or strongly interacting particles, but also factors characterizing the specific DM decay model. We modified the CosmoRec code to include the effect of DM decay and thereby had to take into account additional effects that are not yet included in the Recfast++ runmode of CosmoRec, namely a correction of the photon ionization coefficient and collisional ionizations.

We derived constraints on cosmological parameters using the Planck (2015 release) data [24] including the low- l temperature and polarization likelihood, the high- l TT+TE+EE likelihood and the lensing power spectrum reconstruction likelihood. We find $\lambda > 0.37$ at 95% confidence level for the evolution parameter λ which characterizes the empirical parametrization. We furthermore find that the empirical parametrization allows a much wider range of the spectral index than the CAMB parametrization, namely $n_s = 0.96_{-0.02}^{+0.03}$ (empirical) in contrast to $n_s = 0.965_{-0.007}^{+0.006}$ (CAMB) at 95 % confidence level. On the other hand, the reionization optical depth is tighter constrained in the case of the empirical parametrization, $\tau_{\text{reio}} = 0.05_{-0.010}^{+0.017}$, than in the case of the CAMB parametrization, $\tau_{\text{reio}} = 0.06_{-0.02}^{+0.02}$. This can be explained by the fact that our choice of a flat prior in the evolution parameter λ implies a non-flat prior on the optical depth with a preference of low values of τ_{reio} . Given our lack of knowledge about the value of λ , a flat prior appears reasonable to us. Furthermore the empirical parametrization has an intrinsic prior of $\tau_{\text{reio}} > 0.04$ assuming complete reionization

for $z < 6.1$ which is supported by observations of quasars [40]. We showed that applying a flat prior with $\tau_{\text{reio}} > 0.04$ also in the case of the CAMB parametrization results in a spreading of the likelihood distribution of n_s . The preference of low values of τ_{reio} together with the intrinsic prior on τ_{reio} in the empirical parametrization result in the remarkable broadening of the n_s -likelihood. We conclude that prior knowledge of τ_{reio} is likely to weaken the strong constraints on n_s that were reported in [24]. This can have important consequences for constraining inflationary models.

Turning to the case of DM decay, we find $\Gamma_{\text{eff}} < 2.6 \times 10^{-25} s^{-1}$ using the CAMB parametrization and $\Gamma_{\text{eff}} < 2.9 \times 10^{-25} s^{-1}$ using the empirical parametrization at 95 % confidence level. With an agreement of $\sim 10\%$ we conclude that the constraints of Γ_{eff} are independent of the chosen parametrization of astrophysical reionization. For the electromagnetic decay of a single component DM scenario this translates into $\Gamma < 4.7 \times 10^{-26} s^{-1}$ and $\Gamma < 5.3 \times 10^{-26} s^{-1}$. These constraints are obtained using the on-the-spot approximation (energy emitted by the DM decay immediately absorbed by the medium) and therefore overestimate the effect of DM decay on reionization, more realistic constraints are expected to be weaker. Notably, the likelihood of n_s is also widened for the case of the CAMB parametrization when DM decay is included.

As a specific application of our work, we considered the decay of a keV-mass sterile neutrino which has recently been claimed to be detected at 3.5 keV [35, 36]. To obtain realistic constraints we extended our work beyond the on-the-spot approximation by including a redshift and mass dependent absorption fraction that takes into account the redshifting of the emitted photons [49]. The constraints on the decay rate were reinterpreted in terms of the mass m_s and the mixing angle θ of the sterile neutrino. Our constraints are weaker but on a competitive level with those from the diffuse X-ray [60].

The recent Planck analysis includes robust low- ℓ polarization data and resolves the reionization bump [55, 56]. The new data point to a slightly smaller value of the optical depth ($\tau_{\text{reio}} = 0.58 \pm 0.012$, lollipop+TT) than the previous data ($\tau_{\text{reio}} = 0.63 \pm 0.014$, TT,TE,EE+lowP+lensing) [24]. This is also consistent with our results for the empirical parametrization. Including the improved low- ℓ data will thus give rise to stronger constraints on the effective DM decay rate.

6 Acknowledgements

We are thankful to Jens Chluba for his help with the implementation in CosmoRec, Sebastien Clesse for helpful hints about CosmoMC, Antony Lewis for useful suggestions about sharp edges, Alexander Merle and Aurel Schneider for fruitful discussions about sterile neutrinos. Numerical calculations have been performed using JARA-HPC resources at the RWTH Aachen Compute Cluster. DB acknowledges financial support from CAPES-CSF, grant 8768-13-7, and from the ‘‘Bielefeld Young Researchers’ Fund’’. IMO furthermore acknowledges financial support from Studienstiftung des Deutschen Volkes. We acknowledge support from RTG 1620 ‘‘Models of Gravity’’ funded by DFG.

A Smoothness of visibility function

Within the line-of-sight approach [72], the CMB anisotropies depend not only on the visibility function $g = \dot{\tau}e^{-\tau}$, but also on its first and second derivatives with respect to cosmic time, \dot{g} and \ddot{g} . Therefore, it is important to ensure that the free electron fraction is sufficiently

smooth everywhere. There are two transitions in which discontinuities can appear in our model of the free electron fraction described in sections 2 and 3:

- i) At the transition redshift $z_p = 6.1$ of the empirical parametrization (2.5). To avoid the sharp edge in x_e , we modify the parametrization (2.5) according to ⁶

$$x_e(z) = 1.08 \times \begin{cases} \frac{1-Q_p}{(1+z_p)^3-1} ((1+z_p)^3 - (1+z)^3) + Q_p & \text{for } z < z_p \\ Q_p e^{-\lambda \frac{(z-z_p)^3}{(z-z_p)^2+0.2}} & \text{for } z \geq z_p. \end{cases} \quad (\text{A.1})$$

In figure 2 we show the original parametrization (black lines) and its smoothed version (A.1) (red lines). The smoothing procedure alters the function slightly at all redshifts, but the basic asymptotic behaviour remains the same. Being precise, equation (A.1) still does not have a continuous derivative in a mathematical sense, but it is sufficiently smooth to remove any unphysical spikes as shown in figure 11. We show the visibility function and its first two derivatives, where the solid lines represent the smoothed function and the dotted ones the sharp function. The sharp edge of the original parametrization (2.4) leads to spikes that are most dramatic in the second derivative of the visibility function and can lead to unphysical bias.

- ii) At the transition from recombination to astrophysical reionization (CosmoRec to CAMB modules). For astrophysical reionization histories and using the CAMB parametrization (2.1), the code ensures a smooth transition from recombination to astrophysical reionization. The code uses the output of CosmoRec until a redshift of $z_s = z_{re} + 8\Delta_z$, from where the CAMB code takes on the control of the evolution of the free electron fraction in order to initiate the astrophysical reionization. At this redshift the remaining free electrons from recombination have reached an almost constant level of $\sim 10^{-4}$ and the hyperbolic tangent (2.1) from the astrophysical reionization is still small and flat enough such that the transition is guaranteed to be smooth.

However, for the case of DM decay we cannot use the same procedure, because in this way DM decay is not included at low redshifts. The same also applies to studies of DM annihilation. This is not only undesirable from a physical point of view, but it can also lead to a sharp edge at the transition redshift z_s which in turn leads to unphysical spikes in the derivatives of the visibility function. In order to avoid this problem we start to add up the recombination (CosmoRec) contribution and the reionization (CAMB) contribution at sufficiently high redshifts. This procedure results in a smooth transition, as can be seen in figure 6. But we also have to make sure that the free electron function reaches the correct asymptotic value of 1.16 (assuming double helium ionization), since a simple addition of both contributions would result in higher values. The naive way of setting a minimum condition, i.e. $x_e = \min(1.16, x_e|_{\text{CAMB}} + x_e|_{\text{CosmoRec}})$, would again lead to a sharp feature. We solve this problem by the following smoothing function,

$$x_e = 1.16 \times \left[\tanh \left(\left[\frac{x_e|_{\text{CAMB}} + x_e|_{\text{CosmoRec}}}{1.16} \right]^n \right) \right]^{1/n}, \quad (\text{A.2})$$

where we choose $n = 8$ and which behaves as a simple addition as long as the argument of the hyperbolic tangent is ≤ 1 and then smoothly merges the two contributions to the asymptotic value of 1.16.

⁶A. Lewis, private communication.

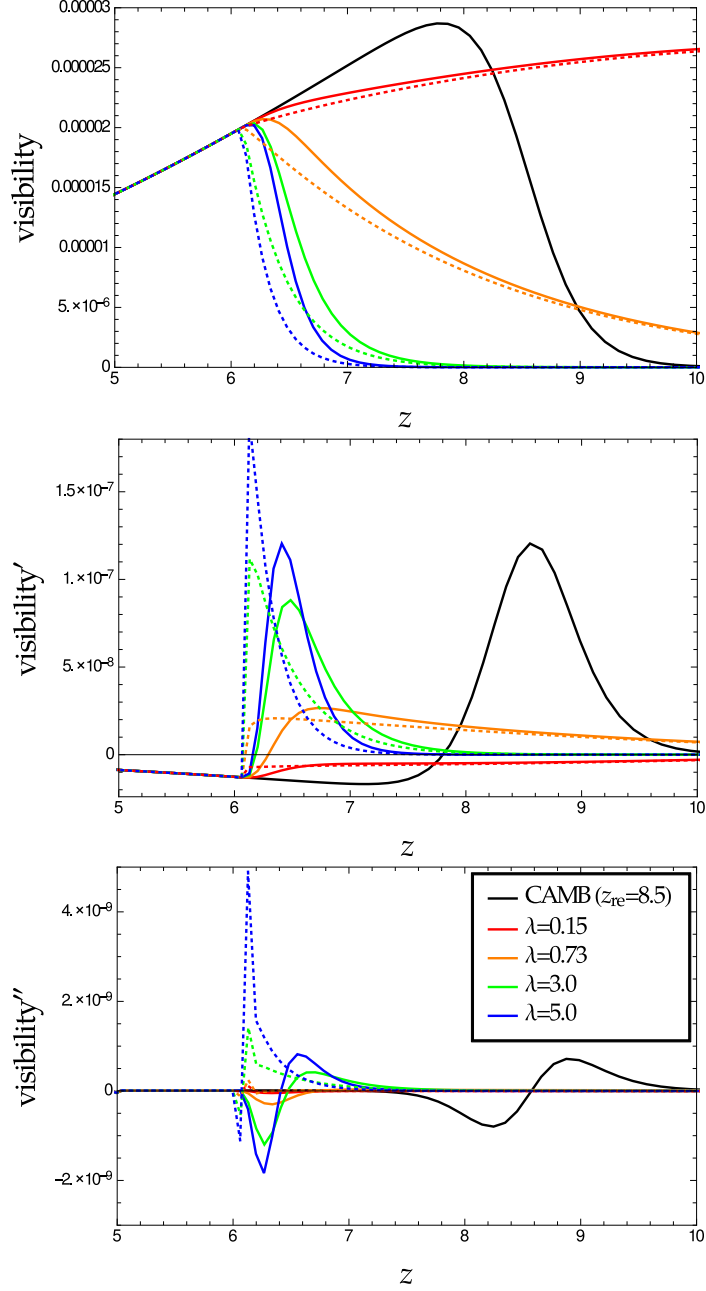


Figure 11: Visibility function (top), its first (middle) and second derivative (bottom) of the empirical parametrization (2.5) for different values of λ , where the dotted curves represent the sharp function (2.4) and the solid curves its smoothed counterpart (A.1). The black curves display the CAMB parametrization for reference.

B Optical depth prior

In this appendix we discuss the different priors on the optical depth imposed by using different parametrizations of reionization, i.e. (2.1) and (2.5), and their implications for the inference of the spectral index n_s . Using a flat prior in λ for the empirical parametrization results in a

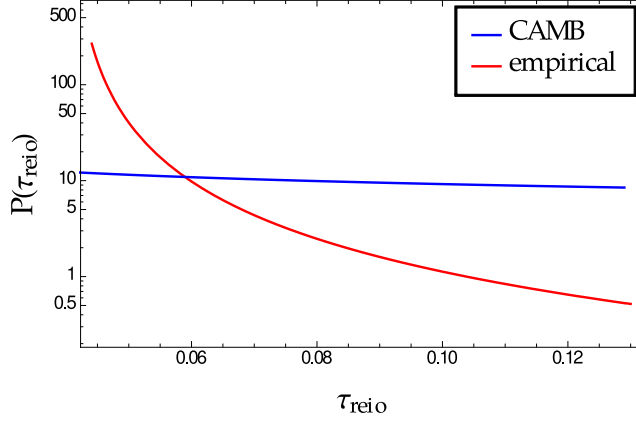


Figure 12: Prior distribution of τ_{reio} implied by a flat prior on z_{re} for the CAMB parametrization (2.1) (blue line) and a flat prior on λ for the empirical parametrization (2.5) (red line) using eq. (B.1).

different prior on τ_{reio} when compared to a flat prior in z_{re} for the CAMB parametrization. The relation between the prior on the optical depth $P(\tau_{\text{reio}})$ and the flat prior \tilde{P} in z_{re} and λ is respectively given by the following relations,

$$P_{\text{CAMB}}(\tau_{\text{reio}}) = \tilde{P}(z_{\text{re}}) \left| \frac{dz_{\text{re}}}{d\tau_{\text{reio}}} \right| \quad \text{and} \quad P_{\text{emp.}}(\tau_{\text{reio}}) = \tilde{P}(\lambda) \left| \frac{d\lambda}{d\tau_{\text{reio}}} \right|. \quad (\text{B.1})$$

In order to find $P_{\text{CAMB}}(\tau_{\text{reio}})$ and $P_{\text{emp.}}(\tau_{\text{reio}})$ we have to derive $z_{\text{re}}(\tau_{\text{reio}})$ and $\lambda(\tau_{\text{reio}})$, which we can obtain by evaluating the integral in (2.6) at $z = z_{\text{rec}}$, i.e., up to the redshift of recombination. For simplicity we hereby neglect the ionization of HeII at redshift ~ 3.5 and furthermore the contribution of the cosmological constant Λ to the Hubble parameter.

For the CAMB parametrization it is convenient to approximate eq. (2.1) by a step-function, which is sufficient to study the leading order dependence of τ_{reio} on z_{re} . We hence find

$$\begin{aligned} \tau_{\text{reio}}|_{\text{CAMB}} &= c\sigma_T \int_0^{z_{\text{rec}}} \frac{n_e(z')}{(1+z')H(z')} dz' \approx \frac{1.08c\sigma_T n_{\text{H},0}}{H_0\sqrt{\Omega_{\text{m}}}} \int_0^{z_{\text{re}}} \sqrt{1+z'} dz' \\ &= \frac{2}{3}\alpha \left[(1+z_{\text{re}})^{3/2} - 1 \right], \end{aligned} \quad (\text{B.2})$$

where we defined $\alpha = \frac{1.08c\sigma_T n_{\text{H},0}}{H_0\sqrt{\Omega_{\text{m}}}}$. This immediately implies

$$\frac{dz_{\text{re}}}{d\tau_{\text{reio}}} \propto \left(\tau_{\text{reio}} + \frac{2}{3}\alpha \right)^{-1/3}. \quad (\text{B.3})$$

For the empirical parametrization we find instead

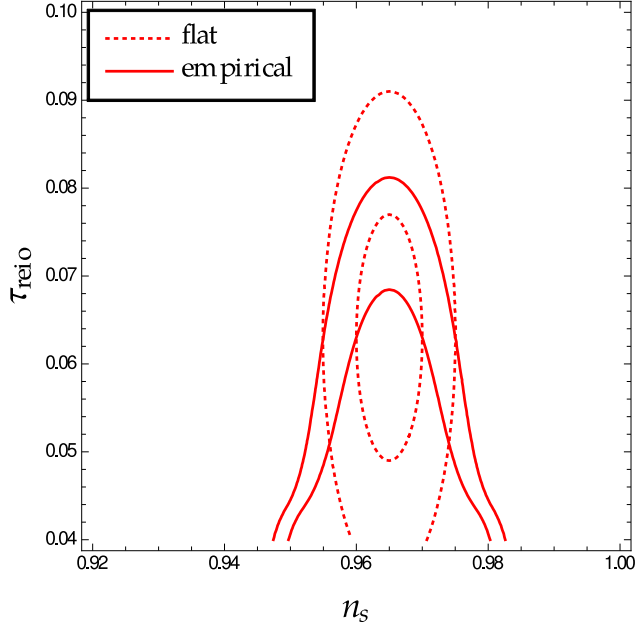


Figure 13: 68% and 95 % confidence contours of a binormal distribution in the $\tau_{\text{reio}}-n_s$ plane (dashed lines). After multiplying with the prior distribution $P_{\text{emp.}}(\tau_{\text{reio}})$ the resulting normalized posterior distribution (solid lines) broadens in n_s direction.

$$\begin{aligned}
 \tau_{\text{reio}}|_{\text{emp.}} &\approx \alpha \left[\int_0^{z_p} \left(\frac{1 - Q_p}{(1 + z_p)^3 - 1} ((1 + z_p)^3 - (1 + z')^3) + Q_p \right) \sqrt{1 + z'} dz' \right. \\
 &\quad \left. + Q_p \int_{z_p}^{\infty} e^{-\lambda(z' - z_p)} \sqrt{1 + z'} dz' \right] \\
 &= \beta + \frac{\alpha Q_p e^{\lambda(1 + z_p)}}{\lambda^{3/2}} \Gamma(3/2, \lambda(1 + z_p)),
 \end{aligned} \tag{B.4}$$

where β is a constant that is simply defined by the first integral in (B.4) and Γ is the incomplete Gamma function. Note that for the second integrand of (B.4) we have approximated $z_{\text{rec}} \rightarrow \infty$. It is possible to differentiate (B.4) with respect to λ analytically, but rewriting the result in terms of τ_{reio} has to be done numerically. In figure 12 we show the priors on τ_{reio} using a flat prior in z_{re} (eq. (B.3)) and a flat prior in λ (eq. (B.4)), taking into account the corresponding normalization.

The empirical parametrization implicitly restricts the optical depth to values $\tau_{\text{reio}} \gtrsim 0.044$, since it assumes (almost) complete ionization for $z \leq z_p = 6.1$. On the other hand, as we can see in figure 12, a flat prior in λ results in a preference for small values of τ_{reio} . The CAMB parametrization instead has a relatively flat prior in τ_{reio} when assuming a flat prior in z_{reio} . This explains why we find much tighter constraints on τ_{reio} when using the empirical parametrization compared to the CAMB parametrization, see figure 7 in section 4.2.

The tight constraints on τ_{reio} in turn result in much weaker constraints on n_s and also A_s , as shown in figure 7. To understand this effect let us for simplicity focus on the $\tau_{\text{reio}} - n_s$ parameter space and neglect the dependence on A_s for the moment. As we show schematically in figure 13 the widening of the posterior distribution is simply caused by normalization. We

show in blue a mock likelihood distribution for τ_{reion} and n_s , assuming a Gaussian normal distribution in both parameters. When multiplying the Gaussian likelihood distribution by the prior distribution $P_{\text{emp.}}(\tau_{\text{reio}})$ (figure 12) and renormalizing accordingly, the posterior distribution gets squeezed into n_s direction.

The same argument holds also in the $\tau_{\text{reio}}-A_s$ plane and we observe the same widening in A_s , see figure 7. However, the difference between the CAMB (2.1) and the empirical parametrization (2.5) in the *marginalized* posterior distribution is much less pronounced for A_s than for n_s . This can be explained by the degeneracy of τ_{reio} with A_s , whereas τ_{reio} and n_s are basically uncorrelated.

References

- [1] J. E. Gunn and B. A. Peterson, “On the Density of Neutral Hydrogen in Intergalactic Space.,” *ApJ* **142** (Nov., 1965) 1633–1641.
- [2] SDSS Collaboration, R. H. Becker *et al.*, “Evidence for reionization at $z \sim 6$: Detection of a Gunn-Peterson trough in a $z = 6.28$ quasar,” *Astron. J.* **122** (2001) 2850, [arXiv:astro-ph/0108097](#) [astro-ph].
- [3] G. Mellema, L. V. E. Koopmans, F. A. Abdalla, G. Bernardi, B. Ciardi, S. Daiboo, A. G. de Bruyn, K. K. Datta, H. Falcke, A. Ferrara, I. T. Iliev, F. Iocco, V. Jelić, H. Jensen, R. Joseph, P. Labropoulos, A. Meiksin, A. Mesinger, A. R. Offringa, V. N. Pandey, J. R. Pritchard, M. G. Santos, D. J. Schwarz, B. Semelin, H. Vedantham, S. Yatawatta, and S. Zaroubi, “Reionization and the Cosmic Dawn with the Square Kilometre Array,” *Experimental Astronomy* **36** (2013) 235–318, [arXiv:1210.0197](#).
- [4] J. C. Pober *et al.*, “What Next-Generation 21 cm Power Spectrum Measurements Can Teach Us About the Epoch of Reionization,” *Astrophys. J.* **782** (2014) 66, [arXiv:1310.7031](#) [astro-ph.CO].
- [5] A. H. Patil *et al.*, “Constraining the epoch of reionization with the variance statistic: simulations of the LOFAR case,” *Mon. Not. Roy. Astron. Soc.* **443** (2014) no. 2, 1113–1124, [arXiv:1401.4172](#) [astro-ph.CO].
- [6] Z. S. Ali *et al.*, “PAPER-64 Constraints on Reionization: The 21cm Power Spectrum at $z = 8.4$,” *Astrophys. J.* **809** (2015) no. 1, 61, [arXiv:1502.06016](#) [astro-ph.CO].
- [7] J. D. Bowman, I. Cairns, D. L. Kaplan, T. Murphy, D. Oberoi, L. Staveley-Smith, W. Arcus, D. G. Barnes, G. Bernardi, F. H. Briggs, S. Brown, J. D. Bunton, A. J. Burgasser, R. J. Cappallo, S. Chatterjee, B. E. Corey, A. Coster, A. Deshpande, L. deSouza, D. Emrich, P. Erickson, R. F. Goeke, B. M. Gaensler, L. J. Greenhill, L. Harvey-Smith, B. J. Hazelton, D. Herne, J. N. Hewitt, M. Johnston-Hollitt, J. C. Kasper, B. B. Kincaid, R. Koenig, E. Kratzenberg, C. J. Lonsdale, M. J. Lynch, L. D. Matthews, S. R. McWhirter, D. A. Mitchell, M. F. Morales, E. H. Morgan, S. M. Ord, J. Pathikulangara, T. Prabu, R. A. Remillard, T. Robishaw, A. E. E. Rogers, A. A. Roshi, J. E. Salah, R. J. Sault, N. U. Shankar, K. S. Srivani, J. B. Stevens, R. Subrahmanyam, S. J. Tingay, R. B. Wayth, M. Waterson, R. L. Webster, A. R. Whitney, A. J. Williams, C. L. Williams, and J. S. B. Wyithe, “Science with the Murchison Widefield Array,” *Publications of the Astronomical Society of Australia* **30** (2013) e031 (28 pages).
- [8] R. A. Monsalve, A. E. E. Rogers, J. D. Bowman, and T. J. Mozdzen, “Calibration of the EDGES Receiver to Observe the Global 21-cm Signature from the Epoch of Reionization,” [arXiv:1602.08065](#) [astro-ph.IM].
- [9] N. Aghanim, F. X. Desert, J. L. Puget, and R. Gispert, “Ionization by early quasars and cosmic microwave background anisotropies,” *Astron. Astrophys.* **311** (1996) 1, [arXiv:astro-ph/9811054](#) [astro-ph]. [*Astron. Astrophys.* 341,640(1999)].

- [10] A. Gruzinov and W. Hu, “Secondary CMB anisotropies in a universe reionized in patches,” *Astrophys. J.* **508** (1998) 435–439, [arXiv:astro-ph/9803188](#) [astro-ph].
- [11] H. M. P. Couchman and M. J. Rees, “Pregalactic evolution in cosmologies with cold dark matter,” *Monthly Notices of the Royal Astronomical Society* **221** (1986) no. 1, 53–62, <http://mnras.oxfordjournals.org/content/221/1/53.full.pdf+html>.
<http://mnras.oxfordjournals.org/content/221/1/53.abstract>.
- [12] J. Miralda-Escude and J. P. Ostriker, “What produces the ionizing background at large redshift?,” *ApJ* **350** (Feb., 1990) 1–22.
- [13] P. Madau, F. Haardt, and M. J. Rees, “Radiative transfer in a clumpy universe. 3. The Nature of cosmological ionizing sources,” *Astrophys. J.* **514** (1999) 648–659, [arXiv:astro-ph/9809058](#) [astro-ph].
- [14] R. Barkana and A. Loeb, “In the beginning: The First sources of light and the reionization of the Universe,” *Phys. Rept.* **349** (2001) 125–238, [arXiv:astro-ph/0010468](#) [astro-ph].
- [15] S. Furlanetto, M. Zaldarriaga, and L. Hernquist, “The Growth of HII regions during reionization,” *Astrophys. J.* **613** (2004) 1–15, [arXiv:astro-ph/0403697](#) [astro-ph].
- [16] N. Y. Gnedin, “Cosmological reionization by stellar sources,” *Astrophys. J.* **535** (2000) 530–554, [arXiv:astro-ph/9909383](#) [astro-ph].
- [17] B. Ciardi, A. Ferrara, and S. D. M. White, “Early reionization by the first galaxies,” *Mon. Not. Roy. Astron. Soc.* **344** (2003) L7, [arXiv:astro-ph/0302451](#) [astro-ph].
- [18] A. Natarajan and D. J. Schwarz, “The effect of early dark matter halos on reionization,” *Phys. Rev.* **D78** (2008) 103524, [arXiv:0805.3945](#) [astro-ph]. [Erratum: *Phys. Rev.* **D81**, 089905(2010)].
- [19] A. Natarajan and D. J. Schwarz, “Distinguishing standard reionization from dark matter models,” *Phys. Rev.* **D81** (2010) 123510, [arXiv:1002.4405](#) [astro-ph.CO].
- [20] J. Chluba, “Could the Cosmological Recombination Spectrum Help Us Understand Annihilating Dark Matter?,” *Mon. Not. Roy. Astron. Soc.* **402** (2010) 1195, [arXiv:0910.3663](#) [astro-ph.CO].
- [21] G. Giesen, J. Lesgourgues, B. Audren, and Y. Ali-Haïmoud, “CMB photons shedding light on dark matter,” *JCAP* **1212** (2012) 008, [arXiv:1209.0247](#) [astro-ph.CO].
- [22] L. Lopez-Honorez, O. Mena, S. Palomares-Ruiz, and A. C. Vincent, “Constraints on dark matter annihilation from CMB observations before Planck,” *JCAP* **1307** (2013) 046, [arXiv:1303.5094](#) [astro-ph.CO].
- [23] V. Poulin, P. D. Serpico, and J. Lesgourgues, “Dark Matter annihilations in halos and the reionization of the universe,” [arXiv:1508.01370](#) [astro-ph.CO].
- [24] **Planck** Collaboration, P. A. R. Ade *et al.*, “Planck 2015 results. XIII. Cosmological parameters,” [arXiv:1502.01589](#) [astro-ph.CO].
- [25] S. Kasuya, M. Kawasaki, and N. Sugiyama, “Partially ionizing the universe by decaying particles,” *Phys. Rev.* **D69** (2004) 023512, [arXiv:astro-ph/0309434](#) [astro-ph].
- [26] E. Pierpaoli, “Decaying particles and the reionization history of the universe,” *Phys. Rev. Lett.* **92** (2004) 031301, [arXiv:astro-ph/0310375](#) [astro-ph].
- [27] S. Kasuya and M. Kawasaki, “Early reionization by decaying particles in light of three year WMAP data,” *JCAP* **0702** (2007) 010, [arXiv:astro-ph/0608283](#) [astro-ph].
- [28] S. Yeung, M. H. Chan, and M. C. Chu, “Cosmic Microwave Background constraints of decaying dark matter particle properties,” *Astrophys. J.* **755** (2012) 108, [arXiv:1206.4114](#) [astro-ph.CO].

- [29] R. Diamanti, L. Lopez-Honorez, O. Mena, S. Palomares-Ruiz, and A. C. Vincent, “Constraining Dark Matter Late-Time Energy Injection: Decays and P-Wave Annihilations,” *JCAP* **1402** (2014) 017, [arXiv:1308.2578 \[astro-ph.CO\]](#).
- [30] F. Iocco, “Dark Matter Capture and Annihilation on the First Stars: Preliminary Estimates,” *Astrophys. J.* **677** (2008) L1–L4, [arXiv:0802.0941 \[astro-ph\]](#).
- [31] K. Freese, P. Gondolo, J. A. Sellwood, and D. Spolyar, “Dark Matter Densities during the Formation of the First Stars and in Dark Stars,” *Astrophys. J.* **693** (2009) 1563–1569, [arXiv:0805.3540 \[astro-ph\]](#).
- [32] M. Mapelli, A. Ferrara, and E. Pierpaoli, “Impact of dark matter decays and annihilations on reionization,” *Mon. Not. Roy. Astron. Soc.* **369** (2006) 1719–1724, [arXiv:astro-ph/0603237 \[astro-ph\]](#).
- [33] H. Liu, T. R. Slatyer, and J. Zavala, “The Darkest Hour Before Dawn: Contributions to Cosmic Reionisation from Dark Matter Annihilation and Decay,” [arXiv:1604.02457 \[astro-ph.CO\]](#).
- [34] R. Adhikari et al., “A White Paper on keV Sterile Neutrino Dark Matter,” [arXiv:1602.04816 \[hep-ph\]](#).
- [35] E. Bulbul, M. Markevitch, A. Foster, R. K. Smith, M. Loewenstein, and S. W. Randall, “Detection of an Unidentified Emission Line in the Stacked X-Ray Spectrum of Galaxy Clusters,” *The Astrophysical J.* **789** (2014) no. 1, 13. <http://stacks.iop.org/0004-637X/789/i=1/a=13>.
- [36] A. Boyarsky, O. Ruchayskiy, D. Iakubovskiy, and J. Franse, “Unidentified Line in X-Ray Spectra of the Andromeda Galaxy and Perseus Galaxy Cluster,” *Phys. Rev. Lett.* **113** (2014) 251301, [arXiv:1402.4119 \[astro-ph.CO\]](#).
- [37] J. Chluba and R. A. Sunyaev, “Induced two-photon decay of the 2s level and the rate of cosmological hydrogen recombination,” *Astron. Astrophys.* **446** (2006) 39–42, [arXiv:astro-ph/0508144 \[astro-ph\]](#).
- [38] J. Chluba and R. M. Thomas, “Towards a complete treatment of the cosmological recombination problem,” *Mon. Not. Roy. Astron. Soc.* **412** (2011) 748, [arXiv:1010.3631 \[astro-ph.CO\]](#).
- [39] M. Douspis, N. Aghanim, S. Ilić, and M. Langer, “A new parameterization of the reionisation history,” *Astron. Astrophys.* **580** (2015) L4, [arXiv:1509.02785 \[astro-ph.CO\]](#).
- [40] R. J. Bouwens, G. D. Illingworth, P. A. Oesch, J. Caruana, B. Holwerda, R. Smit, and S. Wilkins, “Reionization after Planck: The Derived Growth of the Cosmic Ionizing Emissivity now matches the Growth of the Galaxy UV Luminosity Density,” *Astrophys. J.* **811** (2015) no. 2, 140, [arXiv:1503.08228 \[astro-ph.CO\]](#).
- [41] K. Ahn, I. T. Iliev, P. R. Shapiro, G. Mellema, J. Koda, and Y. Mao, “Detecting the Rise and Fall of the First Stars by Their Impact on Cosmic Reionization,” *The Astrophysical Journal Letters* **756** (2012) no. 1, L16. <http://stacks.iop.org/2041-8205/756/i=1/a=L16>.
- [42] H. Park, P. R. Shapiro, E. Komatsu, I. T. Iliev, K. Ahn, and G. Mellema, “The Kinetic Sunyaev-Zel’dovich effect as a probe of the physics of cosmic reionization: the effect of self-regulated reionization,” *Astrophys. J.* **769** (2013) 93, [arXiv:1301.3607 \[astro-ph.CO\]](#).
- [43] M. Kaplinghat, M. Chu, Z. Haiman, G. Holder, L. Knox, and C. Skordis, “Probing the reionization history of the universe using the cosmic microwave background polarization,” *Astrophys. J.* **583** (2003) 24–32, [arXiv:astro-ph/0207591 \[astro-ph\]](#).
- [44] V. Poulin, P. D. Serpico, and J. Lesgourgues, “A fresh look at linear cosmological constraints on a decaying dark matter component,” [arXiv:1606.02073 \[astro-ph.CO\]](#).
- [45] B. Audren, J. Lesgourgues, G. Mangano, P. D. Serpico, and T. Tram, “Strongest

- model-independent bound on the lifetime of Dark Matter,” *JCAP* **1412** (2014) no. 12, 028, [arXiv:1407.2418 \[astro-ph.CO\]](#).
- [46] M. Lattanzi, S. Riemer-Sorensen, M. Tortola, and J. W. F. Valle, “Updated CMB and x- and γ -ray constraints on Majoron dark matter,” *Phys. Rev.* **D88** (2013) no. 6, 063528, [arXiv:1303.4685 \[astro-ph.HE\]](#).
- [47] T. R. Slatyer, “Indirect Dark Matter Signatures in the Cosmic Dark Ages II. Ionization, Heating and Photon Production from Arbitrary Energy Injections,” *Phys. Rev.* **D93** (2016) no. 2, 023521, [arXiv:1506.03812 \[astro-ph.CO\]](#).
- [48] T. R. Slatyer, N. Padmanabhan, and D. P. Finkbeiner, “CMB Constraints on WIMP Annihilation: Energy Absorption During the Recombination Epoch,” *Phys. Rev.* **D80** (2009) 043526, [arXiv:0906.1197 \[astro-ph.CO\]](#).
- [49] E. Ripamonti, M. Mapelli, and A. Ferrara, “Intergalactic medium heating by dark matter,” *Mon. Not. Roy. Astron. Soc.* **374** (2007) 1067–1077, [arXiv:astro-ph/0606482 \[astro-ph\]](#).
- [50] X.-L. Chen and M. Kamionkowski, “Particle decays during the cosmic dark ages,” *Phys. Rev.* **D70** (2004) 043502, [arXiv:astro-ph/0310473 \[astro-ph\]](#).
- [51] J. R. Shaw and J. Chluba, “Precise cosmological parameter estimation using CosmoRec,” *Mon. Not. Roy. Astron. Soc.* **415** (2011) 1343, [arXiv:1102.3683 \[astro-ph.CO\]](#).
- [52] J. Chluba, D. Paoletti, F. Finelli, and J.-A. Rubiño-Martín, “Effect of primordial magnetic fields on the ionization history,” *Mon. Not. Roy. Astron. Soc.* **451** (2015) no. 2, 2244–2250, [arXiv:1503.04827 \[astro-ph.CO\]](#).
- [53] A. Lewis and S. Bridle, “Cosmological parameters from CMB and other data: A Monte Carlo approach,” *Phys. Rev.* **D66** (2002) 103511, [arXiv:astro-ph/0205436 \[astro-ph\]](#).
- [54] A. Lewis, A. Challinor, and A. Lasenby, “Efficient computation of CMB anisotropies in closed FRW models,” *Astrophys. J.* **538** (2000) 473–476, [arXiv:astro-ph/9911177 \[astro-ph\]](#).
- [55] **Planck** Collaboration, N. Aghanim et al., “Planck 2016 intermediate results. XLVI. Reduction of large-scale systematic effects in HFI polarization maps and estimation of the reionization optical depth,” [arXiv:1605.02985 \[astro-ph.CO\]](#).
- [56] **Planck** Collaboration, R. Adam et al., “Planck 2016 intermediate results. XLVII. Planck constraints on reionization history,” [arXiv:1605.03507 \[astro-ph.CO\]](#).
- [57] W. Valkenburg, J. Hamann, and L. M. Krauss, “Effects of Prior Assumptions on Bayesian Estimates of Inflation Parameters, and the expected Gravitational Waves Signal from Inflation,” *Phys. Rev.* **D78** (2008) 063521, [arXiv:0804.3390 \[astro-ph\]](#).
- [58] S. Dodelson and L. M. Widrow, “Sterile-neutrinos as dark matter,” *Phys. Rev. Lett.* **72** (1994) 17–20, [arXiv:hep-ph/9303287 \[hep-ph\]](#).
- [59] S. Tremaine and J. E. Gunn, “Dynamical Role of Light Neutral Leptons in Cosmology,” *Phys. Rev. Lett.* **42** (1979) 407–410.
- [60] A. Boyarsky, A. Neronov, O. Ruchayskiy, and M. Shaposhnikov, “Constraints on sterile neutrino as a dark matter candidate from the diffuse x-ray background,” *Mon. Not. Roy. Astron. Soc.* **370** (2006) 213–218, [arXiv:astro-ph/0512509 \[astro-ph\]](#).
- [61] C. R. Watson, Z.-Y. Li, and N. K. Polley, “Constraining Sterile Neutrino Warm Dark Matter with Chandra Observations of the Andromeda Galaxy,” *JCAP* **1203** (2012) 018, [arXiv:1111.4217 \[astro-ph.CO\]](#).
- [62] A. Boyarsky, A. Neronov, O. Ruchayskiy, M. Shaposhnikov, and I. Tkachev, “Where to find a dark matter sterile neutrino?,” *Phys. Rev. Lett.* **97** (2006) 261302, [arXiv:astro-ph/0603660 \[astro-ph\]](#).
- [63] A. Boyarsky, D. Malyshev, A. Neronov, and O. Ruchayskiy, “Constraining DM properties with

- SPI,” *Mon. Not. Roy. Astron. Soc.* **387** (2008) 1345, [arXiv:0710.4922 \[astro-ph\]](#).
- [64] M. Viel, G. D. Becker, J. S. Bolton, and M. G. Haehnelt, “Warm dark matter as a solution to the small scale crisis: New constraints from high redshift Lyman-alpha forest data,” *Phys. Rev.* **D88** (2013) 043502, [arXiv:1306.2314 \[astro-ph.CO\]](#).
- [65] B. Bozek, M. Boylan-Kolchin, S. Horiuchi, S. Garrison-Kimmel, K. Abazajian, and J. S. Bullock, “Resonant Sterile Neutrino Dark Matter in the Local and High- z Universe,” *Mon. Not. Roy. Astron. Soc.* **459** (2016) 1489, [arXiv:1512.04544 \[astro-ph.CO\]](#).
- [66] A. Schneider, “Astrophysical constraints on resonantly produced sterile neutrino dark matter,” *JCAP* **1604** (2016) no. 04, 059, [arXiv:1601.07553 \[astro-ph.CO\]](#).
- [67] L. V. E. Koopmans *et al.*, “The Cosmic Dawn and Epoch of Reionization with the Square Kilometre Array,” *PoS AASKA14* (2015) 001, [arXiv:1505.07568 \[astro-ph.CO\]](#).
- [68] X.-D. Shi and G. M. Fuller, “A New dark matter candidate: Nonthermal sterile neutrinos,” *Phys. Rev. Lett.* **82** (1999) 2832–2835, [arXiv:astro-ph/9810076 \[astro-ph\]](#).
- [69] A. Merle, V. Niro, and D. Schmidt, “New Production Mechanism for keV Sterile Neutrino Dark Matter by Decays of Frozen-In Scalars,” *JCAP* **1403** (2014) 028, [arXiv:1306.3996 \[hep-ph\]](#).
- [70] A. Merle and M. Totzauer, “keV Sterile Neutrino Dark Matter from Singlet Scalar Decays: Basic Concepts and Subtle Features,” *JCAP* **1506** (2015) 011, [arXiv:1502.01011 \[hep-ph\]](#).
- [71] A. Rudakovskiy and D. Iakubovskiy, “Influence of 7 keV sterile neutrino dark matter on the process of reionization,” *JCAP* **1606** (2016) no. 06, 017, [arXiv:1604.01341 \[astro-ph.CO\]](#).
- [72] U. Seljak and M. Zaldarriaga, “A Line of sight integration approach to cosmic microwave background anisotropies,” *Astrophys. J.* **469** (1996) 437–444, [arXiv:astro-ph/9603033 \[astro-ph\]](#).